

**Title** The role of mitotic cell-substrate adhesion re-modeling in animal cell division.

**Authors**

Christina L. Dix<sup>1\*</sup>, Helen K. Matthews<sup>1\*</sup>, Marina Uroz<sup>3</sup>, Susannah McLaren<sup>1</sup>, Lucie Wolf<sup>2</sup>, Nicholas Heatley<sup>1</sup>, Zaw Win<sup>1</sup>, Pedro Almada<sup>1</sup>, Ricardo Henriques<sup>1</sup>, Michael Boutros<sup>2</sup>, Xavier Trepats<sup>3,4,5,6</sup> and Buzz Baum<sup>1,7</sup>

\*These authors contributed equally

**Affiliations**

<sup>1</sup> MRC - Laboratory for Molecular Cell Biology, University College London, London WC1E 6BT, United Kingdom.

<sup>2</sup> Division of Signaling and Functional Genomics, German Cancer Research Center (DKFZ), and Department for Cell and Molecular Biology, Medical Faculty Mannheim, Heidelberg University, 69120 Heidelberg, Germany

<sup>3</sup> Institute for Bioengineering of Catalonia (IBEC), The Barcelona Institute for Science and Technology (BIST), 08028 Barcelona, Spain

<sup>4</sup> Unitat de Biofísica i Bioenginyeria, Facultat de Medicina, Universitat de Barcelona, 08036 Barcelona, Spain

<sup>5</sup> Institució Catalana de Recerca i Estudis Avançats (ICREA), 08010 Barcelona, Spain

<sup>6</sup> Center for Networked Biomedical Research on Bioengineering, Biomaterials and Nanomedicine (CIBER-BBN), 08028 Barcelona, Spain

<sup>7</sup> Institute for the Physics of Living Systems, University College London, London WC1E 6BT, United Kingdom.

Contact information of lead contact and corresponding author: b.baum@ucl.ac.uk

## **Summary**

Animal cells undergo a dramatic series of shape changes as they divide, which depend on re-modeling of cell-substrate adhesions. Here, we show that while focal adhesion complexes are disassembled during mitotic rounding, integrins remain in place. These integrin-rich contacts connect mitotic cells to the underlying substrate throughout mitosis, guide polarized cell migration following mitotic exit, and are functionally important, since adherent cells undergo division failure when removed from the substrate. Further, the ability of cells to re-spread along pre-existing adhesive contacts is essential for division in cells compromised in their ability to construct a RhoGEF-dependent (Ect2) actomyosin ring. As a result, Ect2 siRNA cells fail to divide on small adhesive islands, but successfully divide on larger patterns, as the connection between daughter cells narrows and severs as they migrate away from one another. In this way, regulated re-modeling of cell-substrate adhesions during mitotic rounding aids cell division in animals.

## **Keywords**

Division, mitotic-rounding, integrin-based adhesion, cytokinesis

## **Introduction**

As animal cells in culture progress through mitosis they undergo a series of changes in shape (reviewed by Ramkumar and Baum, 2016). Most round up as they enter mitosis. They then elongate as they exit mitosis and segregate their DNA, forming a central contractile furrow that narrows around the central spindle to form a mid-body, which is cut during the process of abscission to generate two new daughter cells (reviewed by Fededa and Gerlich, 2012). Two processes are critical for these drastic shape changes to occur efficiently: cells must dynamically re-model both their actomyosin cytoskeleton and the adhesions through which they attach to the substrate.

At the molecular level, the mitotic re-modeling of the actomyosin cytoskeleton is regulated by the RhoGEF Ect2 (Matthews et al., 2012; Miki et al., 1993; Prokopenko et al., 1999; Tatsumoto et al., 1999). Mitotic rounding begins with the export of RhoGEF Ect2 from the nuclear compartment in prophase (Matthews et al., 2012). This activates RhoA (Maddox and Burridge, 2003; Tatsumoto et al., 1999) at the plasma membrane, leading to the construction of a relatively isotropic (Rosa et al., 2015), and mechanically rigid (Kunda et al., 2008; Stewart et al., 2011) actomyosin cortex. At mitotic exit, Ect2 is then recruited to the center of the anaphase spindle (Burkard et al., 2009; Somers and Saint, 2003), to the region of anti-parallel microtubule overlap (Rappaport, 1985), where it activates Rho (Bement et al., 2005; Kimura et al., 2000; Nishimura and Yonemura, 2006; Tatsumoto et al., 1999; Yüce et al., 2005) at the membrane (Kotynová et al., 2016; Wolfe et al., 2009) leading to local actin filament nucleation and Myosin II activation (Su et al., 2011). In combination with signals from anaphase chromatin (Kiyomitsu and Cheeseman, 2013; Rodrigues et al., 2015), these

events polarize the cell cortex (Wagner and Glotzer, 2016), causing cells to undergo cytokinesis as they relax at their poles and constrict at their center (reviewed by Green et al., 2012).

These actomyosin-dependent shape changes can only take place if the adhesive contacts that couple cells to the underlying extracellular matrix are re-modeled upon entry into mitosis ( Dao et al., 2009; Lancaster et al., 2013). While this process is not well-understood, mitotic rounding has been shown to require inactivation of the small GTPase Rap1 (Dao et al., 2009). As a consequence, cells that express a constitutively active form of Rap1 fail to round up properly when they enter mitosis, leading to defects in spindle morphogenesis (Lancaster et al., 2013). Nevertheless, although Rap1 is inactivated at mitotic entry, cells do not lose all contacts with the substrate. Instead, as they round up, cells in culture remain in contact with the substrate through retraction fibres: narrow actin-rich membrane tubes generated during the process of rounding (Mitchison, 1992). In some instances, these retraction fibers have been shown to support significant forces (Fink et al., 2011). Moreover, tension in retraction fibers (Fink et al., 2011) has been shown to guide orientation of the metaphase spindle relative to the pattern of adhesions (Petridou and Skourides, 2016; Théry et al., 2005). These retraction fibers then help guide cell re-spreading as cells exit mitosis and enter G1 (Cramer and Mitchison, 1993).

Here, using hTERT-immortalized RPE1 cells (Bodnar et al., 1998) as a model system in which to investigate the dynamics and function of mitotic adhesion re-modeling, we show that, while most of the components of focal adhesions are lost as cells enter into mitosis, integrins remain in place. The integrin-based contacts that persist throughout

mitosis decorate the portions of the cell that remain attached to the substrate as cell margins retract during mitotic rounding. As a result, they are able to assist in the division process by guiding the rapid re-spreading of cells as they exit mitosis - as evidenced by the fact that mitotic RPE1 cells fail to divide when they are removed from the substrate. This is especially the case in cells with a compromised actomyosin cortex, where mitotic adhesions are essential to enable daughter cells migrating away from one another to undergo abscission, as previously described in *Dictyostelium* and other systems (Kanada et al., 2005, 2008; Nagasaki et al., 2009; Neujahr et al., 1997). Taken together, these data suggest that it is adhesion, not the actomyosin ring, that plays the dominant role in division in adherent non-transformed human cells.

## **Results**

### **Adhesion re-modeling during mitotic cell rounding.**

In order to explore the dynamics of adhesion re-modeling that accompany changes in cell shape during passage through mitosis (reviewed by Ramkumar and Baum, 2016), we chose to image mitotic progression in an adherent, migratory, diploid human cell line: RPE1-hTERT cells (Bodnar et al., 1998), which are widely used to study the cell cycle, cell division, and cell migration in cell culture and as such provide an ideal model for this analysis of mitotic adhesion re-modeling. In these cells, we found that many components of focal adhesions present in interphase were lost upon entry into mitosis (Figure 1A-B). This included Zyxin, which we followed in cells engineered to stably express Zyxin-GFP - a component of the interphase focal adhesion complex (Kanchanawong et al., 2010). The exception to this rule was active  $\beta$ 1-Integrin (Figure 1A), which remained in punctae at the interface between the cell and the substrate throughout mitosis (Lock et al., 2017).

When we used the Zyxin-GFP line to follow adhesion re-modeling live, we saw that, while RPE1 cells were highly motile in interphase, in the minutes prior to entry into mitosis, cells stopped moving, stopped extending lamellipodia, and stopped generating new Zyxin-positive puncta (Figure 1B, 1D). The complete set of Zyxin-positive focal adhesions (and Paxillin puncta (Figure 1A) (Marchesi et al., 2014)) were then rapidly lost as cells rounded up (Figure 1B, 1D), with a timing that varied between puncta (Figure 1E) and between cells (relative to the onset of prometaphase as seen by the influx of GFP into the nucleus due to nuclear envelope permeabilisation (NEP)) (Figure 1C). Despite losing their full complement of focal adhesion complexes, RPE1 cells remained attached to the substrate by thin retraction fibres (Cramer and

Mitchison, 1995; Fink et al., 2011; Théry et al., 2005), and a small number of relatively thick, long linear attachments, which we have called “tails”. 79% of cells exhibited tails, 52% of which were bipolar, with tails aligned along the interphase long cell axis (N =76 cells from 13 experiments).

To explore the path of adhesion re-modeling, we fixed and stained Zyxin-GFP expressing cells that had previously been imaged live (using an online fixation protocol (Almada, 2017)) for active  $\beta$ 1-Integrin. This revealed  $\beta$ 1-Integrin-rich puncta decorating both the retraction fibers and the thicker tails that remained following mitotic rounding - at precisely the same positions as the Zyxin-positive focal adhesions that were lost during prophase (Figure 1F and S1A). This suggests that, as focal adhesion complexes are disassembled during entry into mitosis, they leave behind a stable pool of active  $\beta$ 1-Integrin, which serves as a molecular memory of the adhesion pattern and of interphase cell shape (Lock et al., 2017). We note that adhesion re-modeling was similar in HeLa cells, even though they round without leaving tails (Figure S2A and B) – and is regulated by Rap1 (Lancaster et al., 2013) and essential for cell division (Figure S2C-E).

To assess the function of these substrate attachments, we used the Zyxin-GFP line to track cells as they underwent a complete cycle of rounding and division (Figure 2A). Strikingly, when imaging cells in this way we noted that, although RPE1 cells are high motile and tend to undergo persistent directional migration in interphase, this directionality is erased as cells pass through mitosis (Figure S1B). Instead, the vast majority of daughter cells migrated away from one another following division. This was most evident for cells cultured on micro-patterned lines (Figure S1B-C), but similar

results were seen on non-patterned substrates (data not shown). Strikingly, in these same movies, the focal adhesions disassembled during rounding were reformed at many of the same positions during polar re-spreading in G1 (Figure 2A-B) - as previously described for retraction fibers (Cramer and Mitchison, 1993). At the same time, in line with the data from fixed cells (Figure 1F and S1A), many integrin-based adhesions labelled with ectopically expressed alpha-V-Integrin were retained from mitotic entry to exit (Figure 2C). In addition, daughter cells that adhered well to the substrate throughout mitosis via extensive “tails” re-spread sooner than those that did not (Figure 2D-E). These results demonstrate that cells entering mitosis re-model their focal adhesion complexes to leave integrin-based attachments, which aid daughter cell re-spreading at mitotic exit.

### **The importance of cell-substrate adhesion for RPE1 cell division.**

Having followed adhesion re-modeling during mitotic entry, we wanted to determine whether mitotic cell-substrate adhesion is important for cell division in RPE1 cells. To do so, we followed cells as they progressed through mitosis in the absence of a substrate. Trypsin-EDTA was used to remove cells from a tissue culture dish, which were then plated as single cells into fibronectin-coated control or non-adherent PLL-PEG-coated micro-wells. Importantly, while the lack of adhesion induced cycle arrest in the vast majority of the cells in PEG micro-wells (data not shown), a proportion of cells, presumably those close to the G2/M boundary, were still able to enter mitosis while suspended. Despite undergoing mitotic exit and furrow formation, all of these cells failed to complete abscission (Figure 3A-B). This compares to a failure rate of 11.5% for cells plated in control fibronectin-coated micro-wells (Figure 3B). By contrast, HeLa cells were able to divide in suspension culture under the same conditions (Figure 3C-D). Thus, adhesion is required for a successful division in RPE1 cells, even though they can exit mitosis and form a cytokinetic furrow without it.

To test whether the division failure observed in RPE1 cells passing through mitosis in suspension is due to a functional requirement for adhesion underneath the cytokinetic furrow, we plated cells on ring-shaped adhesive islands. At mitotic exit, the polar regions of these cells re-spread over the perimeter of the adhesive ring, away from the non-adherent division site. And strikingly, all of these cells (11/11 cells in 3 experiments), completed division successfully (Figure S3A), suggesting that cells do not need to establish adhesions under the cytokinetic ring to complete cell division. In line with this conclusion, the region under the furrow was rose up off the substrate as RPE1 cells divided on an adherent substrate (Figure S3B). Furthermore, the rate of

furrow closure was similar in cells dividing on an adhesive structure and over a non-adherent hole (furrow closure on disc  $19.37 \pm 2.32$  nm/sec, N=5 cells. On ring  $18.59 \pm 1.55$  nm/sec, N=3 cells). Thus, while adhesion is required for cell division in RPE1 cells, this does not appear to reflect a requirement for adhesion under the furrow, as had been reported for some other systems (Pellinen et al., 2008).

Since adhesions are sites at which cells exert traction on the substrate, it was also important to test the extent to which traction is required for cell division. When we asked this question by imaging cells dividing on gels of differential stiffness, we saw that, while RPE1 cells were able to divide on an ECM-coated 1.5kPa gel, the majority of cells failed to divide on soft 0.5kPa gels (Figure 3E and S3C). Thus, both cell-substrate adhesion and traction are required for normal RPE1 cell division.

### **Integrin based protrusions allow division in Ect2-depleted cells.**

Having established an important role for adhesion and traction for RPE1 cell division, it is important to determine whether these adhesions are *sufficient* for cell division in the absence of a visible actomyosin ring. While this might seem surprising, since most eukaryotic cells, including in HeLa cells (Figure 4A), require an actomyosin ring for division, which is assembled downstream of the RhoGEF Ect2 and Rho (reviewed by Green et al., 2012), studies using several types of adherent eukaryotic cells, e.g. *Dictyostelium*, NRK and HT1080 fibrosarcoma cells (Kanada et al., 2005, 2008; Nagasaki et al., 2009), have suggested that cells with a compromised actomyosin ring can divide via an alternative mechanism as daughter cells migrate away from one another. To test whether this is also the case for RPE1 cells, we used Ect2 RNAi to compromise formation of an actomyosin ring in cells exiting mitosis (Figure 4B).

Importantly for this analysis, RNAi-mediated silencing of Ect2 was sufficient to deplete cells of the protein (Figure S4A-B), so that Ect2 was no longer visible at the mid-zone of cells exiting mitosis (Figure S4B). While this compromised the assembly of the actomyosin cortex (Figure S4C-E) and mitotic rounding (Figure S4F), as previously reported (Matthews et al., 2012), it did not alter the timing of adhesion re-modeling (Figure S4G-H). Strikingly, 58% of these Ect2-depleted cells divided (N=98 cells from 8 experiments) (Figure 4B). Moreover, the chances of a cell undergoing a successful abscission event without an actomyosin ring, was positively correlated with the presence of adhesive structures linking it to the underlying substrate. Thus, cells with adhesive contacts with the substrate (tails) can divide, while cells without tails tend to fail in division (Figure 4B).

To determine how RPE1 divide even when their ability to form an actomyosin ring is compromised, we used immunofluorescence to examine the set of proteins associated with cytokinesis that are recruited to the cell mid-zone following Ect2 RNAi-mediated silencing. In these cells, levels of F-actin within the neck connecting daughter cells were significantly reduced, relative to the control. In addition, both p-Myosin and Anillin were undetectable from the mid-zone of dividing Ect2 siRNA cells (Figure 4C-D). By contrast, while Aurora B was still recruited to the mid-zone in Ect2 siRNA cells, it was not localized with the same degree of precision as it was in wildtype cells prior to abscission (Figure 4E). Similar results were obtained in live RPE1 cells expressing LifeAct-GFP (Figure 4G). Thus, at anaphase, while control siRNA cells accumulated a central band of actomyosin and formed a narrow furrow, which closed to form the neck that separated the two new daughter cells (Figure 4G-I), before undergoing abscission some time later, as previously described (Fededa and Gerlich, 2012;

Lafaurie-Janvore et al., 2013), division in Ect2 siRNA treated cells occurred in the absence of a visible actomyosin ring or a furrow. Instead, in these cells, the actin cortex was lost from opposing poles as cells exited mitosis (Figure 4G). Then, as daughter cells re-spread and moved away from each other, the connection linking them slowly thinned - culminating in cell division (Figure 4G-I). Similar results were seen in cells treated with a ROCK inhibitor, which compromises actomyosin ring formation (Figure S4I-J; Kanada et al., 2008). Strikingly, this delay in the rate of neck closure in Ect2 siRNA cells did not translate into a delay abscission timing (Figure 4F), which was similar in control and Ect2 RNAi cells. Together these data point to a critical role for mitotic adhesions in the process of division in Ect2-depleted cells.

#### **Re-spreading of daughter cells is required for division in Ect2-depleted cells.**

In these experiments, the ability of daughter cells to migrate away from one another as they exited mitosis appears to determine whether or not they will succeed in dividing. This suggests, in line with work in *Dictyostelium* (Neujahr et al., 1997), that adhesion-dependent migration (Burton and Taylor, 1997) is required to generate the traction forces that allow division in Ect2-depleted cells. As a test of this hypothesis, we constrained daughter cell movement by plating cells on micro-patterns of different sizes. We used patterns of different sizes that were either circular or elliptical in shape (1:2.5 minor: major axis). While control siRNA cells successfully completed division on all patterns (Figure 5A-B top row, and 5C), Ect2 siRNA treated cells tended to fail during division on small, less elongated patterns (Figure 5A middle row and 5C). In cases of division failure, the neck separating daughter cells appeared to narrow as they exited mitosis, before widening again when opposing poles of the re-spreading daughter cells reached the pattern edge (Figure 5A-B middle row). As expected, as

the size and length of patterns was increased, the chances of a successful division began to approach levels seen for cells on non-patterned substrates (Figure 5A-B bottom row, and 5C). Similarly, for cells growing on a non-patterned substrate, the ability of cells to re-spread (measured at 21 minutes after anaphase) was positively correlated with the likelihood of their undergoing a successful division (Figure 5D).

When traction forces were measured, tensile forces were found dropping to baseline levels as cells enter mitosis (Figure S5A-G). This indicates that the adhesive tails that persist through mitosis in RPE1 cells bear almost no tension. At mitotic exit, traction forces are then re-established at cell poles (Figure S5A-G), in opposite directions (Figure S5E-F). By analogy with a tug-of-war, the force acting at the neck can be readily computed as the unbalanced traction exerted at the cell-substrate interface by each of the two daughter cells (Figure S5G). As daughter cells begin to migrate away from each other this force increases, peaking at ~25nN (Figure S5H-J). Strikingly, this is of the order of magnitude as the tugging force between cells undergoing collective migration (Labernadie et al., 2017) and is similar in control and Ect2 RNAi cells (Figure S5J).

Taken together, these data suggest that scission of the physical connection linking migrating daughter cells to one another depends on continuous and polarized lamellipodial extension at opposing daughter cell poles. This generates tension across the connection between daughter cells, narrowing the bridge, enabling abscission in the absence of a visible actomyosin ring. As a test of this idea, we treated cells with a small molecule, the Arp2/3 inhibitor CK666 (Nolen et al., 2009), which inhibits lamellipodial formation and adhesion-dependent cell migration. While few cells

entered mitosis in the presence of the Arp2/3 inhibitor, those Ect2 RNAi cells that entered and progressed through mitosis failed to narrow the region between daughter cells. Instead, they simply re-spread as large binuclear cells (Figure 5E); supporting the idea that Arp2/3 dependent migration is required for division under these conditions.

Finally, to determine whether Ect2-depleted cells require adhesions and retraction fibers laid down during mitotic rounding to divide, we removed control and Ect2 RNAi cells that had been arrested in mitosis from the substrate. Cells were then re-plated on fibronectin and followed as they re-spread and exited mitosis. Strikingly, while almost all control siRNA cells successfully divided under these conditions, the vast majority of Ect2 siRNA cells failed (Figure 5F). This suggests that it is the cell-substrate contacts left during the adhesion re-modeling process that accompanies mitotic rounding which guide adhesion-mediated division in cells compromised in their ability to construct an actomyosin ring. Similarly, when we grew cells on a non-specific adhesive substrate, PLL, to prevent the formation of tails during mitotic rounding, the vast majority of Ect2 RNAi cells failed in division (Figure 5G).

## **Discussion**

In this study, we present a detailed analysis of the dynamics and function of mitotic adhesion re-modeling. This reveals a role for the adhesions laid down upon entry into mitosis in cell division both in cells with a normal actomyosin cortex and in those that lack a contractile actomyosin ring. Importantly, our data suggest that in order to undergo division in the absence of a visible contractile ring, RPE1 cells must retain the adhesions generated during mitotic rounding, since Ect2 RNAi cells fail to divide when they are re-plated from suspension in metaphase onto an adhesive structure and allowed to exit mitosis. This is possible because, while the peripheral proteins normally associated with focal adhesion complexes dissociate from cell-substrate adhesions during the process of rounding, stable active  $\beta$ 1-Integrin puncta remain; decorating retraction fibers and tails that connect the cell to the substrate (Figure 1 and Figure 6A). These adhesions then guide spindle orientation (Fink et al., 2011; Théry et al., 2005), and aid daughter cell re-spreading (Cramer and Mitchison, 1993) and cell division (Figure 3A-B, and Figure 6B). In addition, in cells with a compromised actomyosin cortex, these integrin-based adhesions are absolutely essential for cell division, as was shown to be the case for cell-substrate adhesion in *Dictyostelium* and some other systems (Neujahr et al., 1997; Nagasaki et al., 2002; Kanada et al., 2005, 2008; Nagasaki et al., 2009). In line with a role for mitotic adhesions in this process, HeLa Kyoto cells, which fail to generate long adherent tail-like structures when they round up and enter mitosis (Matthews et al., 2012), fail to divide following Ect2 siRNA, but can be induced to undergo adhesion-dependent division through the expression of an activated form of Rap1 (Figure S5K and Figure 6C I and II).

Most animal cells appear to use an Ect2-dependent actomyosin-based cytokinetic ring to close the plasma membrane around the spindle, leading to a V-shaped neck, which provides a substrate for mid-body assembly and abscission. By contrast, when undergoing an adhesion-dependent division, RPE1 cells do not assemble a visible actomyosin ring, do not accumulate Anillin and pMyosin II at the future division site, and do not form a V-shaped neck as they divide. Instead, as daughter cells move away from one another, the bridge connecting RPE1 sisters slowly thins as the result of traction forces generated by the polar migration of daughter cells away from one another. A morphologically similar division through daughter cell migration has been reported for NRK and HT1080 fibrosarcoma cells (Kanada et al., 2005) treated with 30 $\mu$ M blebbistatin, and a similar migration-based division mechanism has been reported to enable multinucleate cells in interphase to undergo fission in interphase (Ben-Ze'ev and Raz, 1981). When sufficiently thin, this membrane bridge likely forms a good substrate for the abscission machinery. Thus, adhesion-dependent division is likely to be a general phenomenon that relies on the transmission of traction forces from the leading edge of polarized migrating cells to the bridge.

In *Dictyostelium*, the forces driving adhesion-based cell division depend on the polarized activity of the Arp2/3 activator, SCAR/WAVE (King et al., 2010). Similarly, in our system, cell division in the absence of a visible Ect2-based actomyosin ring depends on Arp2/3. In this, our work parallels recent developments in the field of cell migration, where it has recently become clear that there are a variety of mechanisms by which cells can move. Thus, it has been proposed that cells can use polarized Rho activity to *squeeze* themselves forward or can use polarized Rac1 activity and adhesion to *pull* themselves forward (Lämmermann and Sixt, 2009; Sanz-Moreno and

Marshall, 2010). In a similar manner, we suggest that dividing cells can use high Rho activity and Formin-nucleated actomyosin assemblies to *squeeze* daughter cells apart (Figure 6A\*), or can employ Rac1, SCAR/WAVE and Arp2/3 activity together with adhesion to generate directional traction forces to *pull* daughter cells apart (Figure 6C\*\*).

How then does abscission occur in these conditions? First tensions must be transmitted across the dividing cell to thin the connection linking daughter cells. How this occurs requires further investigation. One possibility, however, is that cytokinesis relies on membrane tension-dependent signaling from the lamellipodium to the cell rear as previously described for migrating cells (Diz-Muñoz et al., 2016). Interestingly, in HeLa cells, the movement of daughter cells away from one another following mitotic exit has been shown to delay rather than aid cell separation (Lafaurie-Janvore et al., 2013). This, the authors suggested, is a result of tensile forces across the bridge connecting daughter cells inhibiting ESCRTIII-mediated abscission (Lafaurie-Janvore et al., 2013); an effect that may be due in part to the effect of tension on the actomyosin cortex in the bridge (Figure 2H and Lafaurie-Janvore et al., 2013), since actin can inhibit abscission if it is not cleared from the mid-body region in a timely manner (Echard, 2012). These data imply that assembly of the mid-body during the process of ring contraction (Hu et al., 2012) functions to inhibit abscission until the appropriate time, when Spastin and the ESCRTIII machinery are recruited to induce abscission at a nearby site (Connell et al., 2009; Guizetti et al., 2011). This may be an important feature of many systems, e.g. epithelia, where connections between daughter cells should be established prior to abscission in order to prevent tissue disruption (Herszterg et al., 2013). It may also make the system subject to checkpoint-mediated

control (Norden et al., 2006; Steigemann et al., 2009). However, as we show in this paper, efficient abscission does not absolutely require a well-structured mid-body formed through cortical ring contraction, since abscission time is not impaired in Ect2-depleted cells (Figure 3H and S3D). Moreover, as we show, stretching of the bridge (which we note contains Aurora B) appears to be essential for division in RPE1 cells that lack an actomyosin ring. These considerations make it clear that the primary goal of cytokinesis is to thin the bridge connecting the daughter cells so that it is sufficiently narrow to provide a good substrate for the abscission machinery (Guizetti et al., 2011; Mierzwa and Gerlich, 2014).

Finally, this study highlights two different types of division system in human cells in culture. Transformed cells, like HeLa cells, tend to be very good at mitotic rounding (Matthews and Baum, 2012), likely as a result of having relatively weak cell-substrate adhesion at mitotic entry and a highly contractile cortical actomyosin network. As a consequence, these cells are unable to use adhesions as an aid to division. Instead, like divisions in the zygote, they rely on cell autonomous cues to position Ect2 and to assemble a robust contractile actomyosin ring to divide – making them an ideal system in which to study actomyosin ring formation and function (Bodnar et al., 1998; Kotynová et al., 2016; Matthews et al., 2012). As a result, HeLa cells divide in a manner that is relatively independent of their environment, e.g. in suspension (Figure 3C-D) and/or in soft agar (Cox, 1997). In line with this, in a previous study V12 H-Ras-transformed fibroblasts succeeded to divide in suspension whereas control cells did not (Thullberg et al., 2007), suggesting oncogenic signaling may itself help override the requirement for adhesion; perhaps by increasing cortical tension. By contrast, as our study makes clear, adherent non-transformed RPE1 cells, rely on interactions with the extracellular environment to divide. As a result, while they are unable to divide in

suspension, they are able to use adhesive contacts with their environment to divide under other conditions. Moreover, because RPE1 cells tend to round relatively little when they enter mitosis, they are very good at using adhesive cues in the environment to guide spindle positioning (Théry et al., 2005). While more work must be done before one can conclude that these findings represent a general mechanistic difference between normal and cancer cells divisions (as discussed in Matthews and Baum, 2012), this may go some way towards explaining the differences between cells that divide using an autonomous actomyosin ring, which maybe a general feature of metastatic cancer cell divisions (reviewed by Matthews and Baum, 2012), and adhesion-based cell division mechanisms (Kanada et al., 2005, 2008; Nagasaki et al., 2009; Neujahr et al., 1997) that rely on intimate contact between a cell and its extracellular environment. If so, it will be important in future work to explore the crosstalk between adhesion and cortical contractility in normal and cancer cells.

### **Acknowledgements:**

The author confirms that there are no conflicts of interest. C.D. was supported by PhD funding from the Medical Research Council (UK). H.K.M. was supported by Cancer research UK (CRUK) grant number C1529/A17343 and on a CRUK/EPSRC MDPA grant (C1529/A23335). M.U. was funded by a grant from the Spanish Ministry of Economy and Competitiveness/FEDER (BES-2013-062633). L.W. was funded by a grant from the Deutsche Forschungsgemeinschaft (DFG) RTG2099 “Hallmarks of Skin Cancer.” R.H. and P.A. research supported by grants from the UK BBSRC (BB/M022374/1; BB/P027431/1; BB/R000697/1) and UK MRC (MR/K015826/1). The authors should like to thank Martial Ballard, Matthieu Piel, Nitya Ramkumar and Jeremy Carlton for useful comments on the text.

### **Author contributions:**

C.D.\* conceived and carried out experiments, and wrote manuscript.

H.K.M.\* conceived work and carried out micro-well experiments.

M.U. carried out traction force microscopy and soft gels experiments.

S.M. carried out micro-patterning experiments.

L.W. carried out micro-patterning experiments.

N.H. carried out live and fixed imaging in HeLa with and without Rap1 Q63E.

Z.W. carried out RPE1 migration on lines experiments.

P.A. carried out on online fixation experiment with C.D.

R.H. helped oversee online fixation experiment.

X.T. helped oversee work of M.U.

M.B. helped oversee work of L.W.

B.B. helped to conceive and oversee work and writing.

### **Declaration of interests**

The authors declare no competing interests

## **References**

- Almada, P. (2017). Developing Highly Multiplexed Technology for High-throughput Super-resolution Fluorescence Microscopy. University College London.
- Bement, W.M., Benink, H.A., and Von Dassow, G. (2005). A microtubule-dependent zone of active RhoA during cleavage plane specification. *J. Cell Biol.* 170, 91–101.
- Ben-Ze'ev, A., and Raz, A. (1981). Multinucleation and inhibition of cytokinesis in suspended cells: Reversal upon reattachment to a substrate. *Cell* 26, 107–115.
- Bodnar, A.G., Ouellette, M., Frolkis, M., Holt, S.E., Chiu, C.-P., Morin, G.B., Harley, C.B., Shay, J.W., Lichtsteiner, S., and Wright, W.E. (1998). Extension of Life-Span by Introduction of Telomerase into Normal Human Cells. *Science.* 279, 349–352.
- Burkard, M.E., Maciejowski, J., Rodriguez-Bravo, V., Repka, M., Lowery, D.M., Clauser, K.R., Zhang, C., Shokat, K.M., Carr, S.A., Yaffe, M.B., et al. (2009). Plk1 self-organization and priming phosphorylation of HsCYK-4 at the spindle midzone regulate the onset of division in human cells. *PLoS Biol.* 7, e1000111.
- Burton, K., and Taylor, D.L. (1997). Traction forces of cytokinesis measured with optically modified elastic substrata. *Nature* 385, 450–454.
- Connell, J.W., Lindon, C., Luzio, J.P., and Reid, E. (2009). Spastin couples microtubule severing to membrane traffic in completion of cytokinesis and secretion. *Traffic* 10, 42–56.
- Cox, G.S. (1997). Correlation in HeLa Cells of Anchorage-Independent Growth and Synthesis of the Glycoprotein Hormone  $\alpha$ -Subunit. *Biochem. Biophys. Res. Commun.* 233, 425–431.
- Cramer, L.P., and Mitchison, T.J. (1993). Moving and stationary actin filaments are involved in spreading of postmitotic PtK2 cells. *J. Cell Biol.* 122, 833–843.
- Cramer, L.P., and Mitchison, T.J. (1995). Myosin is involved in postmitotic cell

spreading. *J. Cell Biol.* *131*, 179–189.

Dao, V.T., Dupuy, A.G., Gavet, O., Caron, E., and de Gunzburg, J. (2009). Dynamic changes in Rap1 activity are required for cell retraction and spreading during mitosis. *J. Cell Sci.* *122*, 2996–3004.

Diz-Muñoz, A., Thurley, K., Chintamen, S., Altschuler, S.J., Wu, L.F., Fletcher, D.A., and Weiner, O.D. (2016). Membrane Tension Acts Through PLD2 and mTORC2 to Limit Actin Network Assembly During Neutrophil Migration. *PLoS Biol.* *14*, 1–30.

Dupuy, A.G., L’Hoste, S., Cherfils, J., Camonis, J., Gaudriault, G., and De Gunzburg, J. (2005). Novel Rap1 dominant-negative mutants interfere selectively with C3G and Epac. *Oncogene* *24*, 4509–4520.

Echard, A. (2012). Connecting membrane traffic to ESCRT and the final cut. *Nat. Cell Biol.* *14*, 983–985.

Fededa, J.P., and Gerlich, D.W. (2012). Molecular control of animal cell cytokinesis. *Nat Cell Biol* *14*, 440–447.

Fink, J., Carpi, N., Betz, T., Bétard, A., Chebah, M., Azioune, A., Bornens, M., Sykes, C., Fetler, L., Cuvelier, D., et al. (2011). External forces control mitotic spindle positioning. *Nat. Cell Biol.* *13*, 771–778.

Franco, S.J., Rodgers, M.A., Perrin, B.J., Han, J., Bennin, D.A., Critchley, D.R., and Huttenlocher, A. (2004). Calpain-mediated proteolysis of talin regulates adhesion dynamics. *Nat. Cell Biol.* *6*, 977–983.

Green, R.A., Paluch, E., and Oegema, K. (2012). Cytokinesis in Animal Cells. *Annu. Rev. Cell Dev. Biol.* *28*, 29–58.

Guizetti, J., Schermelleh, L., Mäntler, J., Maar, S., Poser, I., Leonhardt, H., Müller-Reichert, T., and Gerlich, D.W. (2011). Cortical Constriction During Abscission Involves Helices of ESCRT-III-Dependent Filaments. *Science.* *331*, 1616–1620.

Herszterg, S., Leibfried, A., Bosveld, F., Martin, C., and Bellaiche, Y. (2013). Interplay between the Dividing Cell and Its Neighbors Regulates Adherens Junction Formation during Cytokinesis in Epithelial Tissue. *Dev. Cell* 24, 256–270.

Hu, C., Coughlin, M., and Mitchison, T.J. (2012). Midbody assembly and its regulation during cytokinesis. *Mol. Biol. Cell* 23, 1024–1034.

Hu, C.K., Coughlin, M., Field, C.M., and Mitchison, T.J. (2008). Cell polarization during monopolar cytokinesis. *J. Cell Biol.* 181, 195–202.

Hutchins, J.R. a, Toyoda, Y., Hegemann, B., Poser, I., Sykora, M.M., Augsburg, M., Hudecz, O., Buschhorn, B. a, Bulkescher, J., Conrad, C., et al. (2010). Systematic Characterization of Human Protein Complexes Identifies Chromosome Segregation Proteins. *Science*. 328, 593–599.

Kanada, M., Nagasaki, A., and Uyeda, T.Q. (2005). Adhesion-dependent and Contractile Ring-independent Equatorial Furrowing during Cytokinesis in Mammalian Cells. *Mol. Biol. Cell* 16, 3865–3872.

Kanada, M., Nagasaki, A., and Uyeda, T.Q.P. (2008). Novel Functions of Ect2 in Polar Lamellipodia Formation and Polarity Maintenance during “Contractile Ring-Independent” Cytokinesis in Adherent Cells. *Mol. Biol. Cell* 19, 308–317.

Kanchanawong, P., Shtengel, G., Pasapera, A.M., Ramko, E.B., Davidson, W., Hess, H.F., and Waterman, C.M. (2010). Nanoscale architecture of integrin-based cell adhesions. *Nature* 468, 580–584.

Kimura, K., Tsuji, T., Takada, Y., Miki, T., and Narumiya, S. (2000). Accumulation of GTP-bound RhoA during cytokinesis and a critical role of ECT2 in this accumulation. *J. Biol. Chem.* 275, 17233–17236.

King, J.S., Veltman, D.M., Georgiou, M., Baum, B., and Insall, R.H. (2010). SCAR/WAVE is activated at mitosis and drives myosin-independent cytokinesis. *J.*

Cell Sci. *123*, 2246–2255.

Kiyomitsu, T., and Cheeseman, I.M. (2013). Cortical Dynein and asymmetric membrane elongation coordinately position the spindle in anaphase. *Cell* *154*, 391–402.

Kotynová, K., Su, K.C., West, S.C., and Petronczki, M. (2016). Plasma Membrane Association but Not Midzone Recruitment of RhoGEF ECT2 Is Essential for Cytokinesis. *Cell Rep.* *17*, 2672–2686.

Kunda, P., Pelling, A.E., Liu, T., and Baum, B. (2008). Moesin Controls Cortical Rigidity, Cell Rounding, and Spindle Morphogenesis during Mitosis. *Curr. Biol.* *18*, 91–101.

Labernadie, A., Kato, T., Brugués, A., Serra-Picamal, X., Derzsi, S., Arwert, E., Weston, A., González-Tarragó, V., Elosegui-Artola, A., Albertazzi, L., et al. (2017). A mechanically active heterotypic E-cadherin/N-cadherin adhesion enables fibroblasts to drive cancer cell invasion. *Nat. Cell Biol.* *19*, 224.

Lafaurie-Janvore, J., Maiuri, P., Wang, I., Pinot, M., Manneville, J.-B., Betz, T., Balland, M., and Piel, M. (2013). ESCRT-III Assembly and Cytokinetic Abscission Are Induced by Tension Release in the Intercellular Bridge. *Science*. *339*, 1625–1629.

Lämmermann, T., and Sixt, M. (2009). Mechanical modes of “amoeboid” cell migration. *Curr. Opin. Cell Biol.* *21*, 636–644.

Lancaster, O.M., Le Berre, M., Dimitracopoulos, A., Bonazzi, D., Zlotek-Zlotkiewicz, E., Picone, R., Duke, T., Piel, M., and Baum, B. (2013). Mitotic Rounding Alters Cell Geometry to Ensure Efficient Bipolar Spindle Formation. *Dev. Cell* *25*, 1–14.

Laukaitis, C.M., Webb, D.J., Donais, K., and Horwitz, A.F. (2001). Differential dynamics of  $\alpha 5$  integrin, paxillin, and  $\alpha$ -actinin during formation and disassembly of

adhesions in migrating cells. *J. Cell Biol.* *153*, 1427–1440.

Lock, J.G., Jones, M.C., Askari, J.A., Gong, X., Oddone, A., Olofsson, H., Göransson, S., Lakadamyali, M., Humphries, M.J., and Strömblad, S. (2017). Reticular adhesions: A new class of adhesion complex that mediates cell-matrix attachment during mitosis. *BioArchiv*.

Maddox, A.S., and Burridge, K. (2003). RhoA is required for cortical retraction and rigidity during mitotic cell rounding. *J. Cell Biol.* *160*, 255–265.

Marchesi, S., Montani, F., Deflorian, G., D’Antuono, R., Cuomo, A., Bologna, S., Mazzoccoli, C., Bonaldi, T., Di Fiore, P.P., and Nicassio, F. (2014). DEPDC1B Coordinates De-adhesion Events and Cell-Cycle Progression at Mitosis. *Dev. Cell* *31*, 420–433.

Matthews, H.K., and Baum, B. (2012). The metastatic cancer cell cortex: An adaptation to enhance robust cell division in novel environments? *BioEssays* *34*, 1017–1020.

Matthews, H.K., Delabre, U., Rohn, J.L., Guck, J., Kunda, P., and Baum, B. (2012). Changes in Ect2 localization couple actomyosin-dependent cell shape changes to mitotic progression. *Dev. Cell* *23*, 371–383.

Mierzwa, B., and Gerlich, D.W. (2014). Cytokinetic Abscission: Molecular Mechanisms and Temporal Control. *Dev. Cell* *31*, 525–538.

Miki, T., Smith, C.L., Long, J.E., Eva, A., and Fleming, T.P. (1993). Oncogene *ect2* is related to regulators of small GTP-binding proteins. *Nature* *362*, 462–465.

Mitchison, T.J. (1992). Actin based motility on retraction fibers in mitotic PtK2 cells. *Cell Motil. Cytoskeleton* *22*, 135–151.

Nagasaki, A., de Hostos, E.L., and Uyeda, T.Q.P. (2002). Genetic and morphological evidence for two parallel pathways of cell-cycle-coupled cytokinesis in *Dictyostelium*.

J. Cell Sci. 115, 2241–2251.

Nagasaki, A., Kanada, M., and Uyeda, T.Q. (2009). Cell adhesion molecules regulate contractile ring-independent cytokinesis in *Dictyostelium discoideum*. Cell Res. 19, 236–246.

Neujahr, R., Heizer, C., and Gerisch, G. (1997). Myosin II-independent processes in mitotic cells of *Dictyostelium discoideum*: redistribution of the nuclei, re-arrangement of the actin system and formation of the cleavage furrow. J. Cell Sci. 110, 123–137.

Nishimura, Y., and Yonemura, S. (2006). Centralspindlin regulates ECT2 and RhoA accumulation at the equatorial cortex during cytokinesis. J. Cell Sci. 119, 104–114.

Nolen, B.J., Tomasevic, N., Russell, A., Pierce, D.W., Jia, Z., McCormick, C.D., Sakowicz, R., and Pollard, T.D. (2009). Characterization of two classes of small molecule inhibitors of Arp2/3 complex. Nature 460, 1031–1034.

Norden, C., Mendoza, M., Dobbelaere, J., Kotwaliwale, C. V., Biggins, S., and Barral, Y. (2006). The NoCut Pathway Links Completion of Cytokinesis to Spindle Midzone Function to Prevent Chromosome Breakage. Cell 125, 85–98.

Pellinen, T., Tuomi, S., Arjonen, A., Wolf, M., Edgren, H., Meyer, H., Grosse, R., Kitzing, T., Rantala, J.K., Kallioniemi, O., et al. (2008). Integrin trafficking regulated by Rab21 is necessary for cytokinesis. Dev. Cell 15, 371–385.

Petridou, N.I., and Skourides, P.A. (2016). A ligand-independent integrin  $\beta 1$  mechanosensory complex guides spindle orientation. Nat. Commun. 7, 10899.

Prokopenko, S.N., Brumby, A., O’Keefe, L., Prior, L., He, Y., Saint, R., and Bellen, H.J. (1999). A putative exchange factor for Rho1 GTPase is required for initiation of cytokinesis in *Drosophila*. Genes Dev. 13, 2301–2314.

Ramkumar, N., and Baum, B. (2016). Coupling changes in cell shape to chromosome segregation. Nat. Re 17, 511–521.

Rappaport, R. (1985). Repeated furrow formation from a single mitotic apparatus in cylindrical sand dollar eggs. *J. Exp. Zool.* *234*, 167–171.

Rodrigues, N.T.L., Lekomtsev, S., Jananji, S., Kriston-Vizi, J., Hickson, G.R.X., and Baum, B. (2015). Kinetochore-localized PP1–Sds22 couples chromosome segregation to polar relaxation. *Nature* *524*, 489–492.

Rosa, A., Vlassaks, E., Pichaud, F., and Baum, B. (2015). Ect2 / Pbl Acts via Rho and Polarity Proteins to Direct the Assembly of an Isotropic Actomyosin Cortex upon Mitotic Entry. *Dev. Cell* *32*, 1–13.

Sanz-Moreno, V., and Marshall, C.J. (2010). The plasticity of cytoskeletal dynamics underlying neoplastic cell migration. *Curr. Opin. Cell Biol.* *22*, 690–696.

Somers, W.G., and Saint, R. (2003). A RhoGEF and Rho family GTPase-activating protein complex links the contractile ring to cortical microtubules at the onset of cytokinesis. *Dev. Cell* *4*, 29–39.

Steigemann, P., Wurzenberger, C., Schmitz, M.H.A., Held, M., Guizetti, J., Maar, S., and Gerlich, D.W. (2009). Aurora B-Mediated Abscission Checkpoint Protects against Tetraploidization. *Cell* *136*, 473–484.

Stewart, M.P., Helenius, J., Toyoda, Y., Ramanathan, S.P., Muller, D.J., and Hyman, A.A. (2011). Hydrostatic pressure and the actomyosin cortex drive mitotic cell rounding. *Nature* *469*, 226–230.

Su, K.C., Takaki, T., and Petronczki, M. (2011). Targeting of the RhoGEF Ect2 to the Equatorial Membrane Controls Cleavage Furrow Formation during Cytokinesis. *Dev. Cell* *21*, 1104–1115.

Tatsumoto, T., Xie, X., Blumenthal, R., Okamoto, I., and Miki, T. (1999). Human ECT2 is an exchange factor for Rho GTPases, phosphorylated in G2/M phases, and involved in cytokinesis. *J. Cell Biol.* *147*, 921–927.

Théry, M., Racine, V., Pépin, A., Piel, M., Chen, Y., Sibarita, J.-B., and Bornens, M. (2005). The extracellular matrix guides the orientation of the cell division axis. *Nat. Cell Biol.* *7*, 947–953.

Thullberg, M., Gad, A., Guyader, S. Le, Stro, S., Le Guyader, S., and Strömblad, S. (2007). Oncogenic H-Ras V12 promotes anchorage-independent cytokinesis in human fibroblasts *Minna*. *Proc. Natl. Acad. Sci. U. S. A.* *104*, 20338–20343.

Trepat, X., Wasserman, M.R., Angelini, T.E., Millet, E., Weitz, D.A., Butler, J.P., and Fredberg, J.J. (2009). Physical forces during collective cell migration. *Nat. Phys.* *5*, 426–430.

Wagner, E., and Glotzer, M. (2016). Local RhoA activation induces cytokinetic furrows independent of spindle position and cell cycle stage. *J. Cell Biol.* *213*, 641–649.

Welman, A., Serrels, A., Brunton, V.G., Ditzel, M., and Frame, M.C. (2010). Two-color photoactivatable probe for selective tracking of proteins and cells. *J. Biol. Chem.* *285*, 11607–11616.

Wolfe, B.A., Takaki, T., Petronczki, M., and Glotzer, M. (2009). Polo-like kinase 1 directs assembly of the HsCyk-4 RhoGAP/Ect2 RhoGEF complex to initiate cleavage furrow formation. *PLoS Biol.* *7*, e1000110.

Yüce, Ö., Piekny, A., and Glotzer, M. (2005). An ECT2-centralspindlin complex regulates the localization and function of RhoA. *J. Cell Biol.* *170*, 571–582.

## **Figure legends**

**Figure 1.** Adhesion re-modeling during mitotic cell rounding:

**(A)** Images depict fixed RPE1 cells in interphase and metaphase stained for Talin, active  $\beta 1$ -Integrin (magenta) and Paxillin (yellow). Merge also shows DAPI (blue). 1 basal z-slice. Scale-bar 20  $\mu\text{m}$ . **(B)** Graph showing loss of Zyxin-positive adhesion sites as cells progress through mitosis. N=10 cells from 7 experiments. Mean  $\pm$  SD. **(C)** Graphs show adhesion loss relative to NEP in 6 sample cells at mitotic entry. **(D)** Image depicts adhesion re-modeling in a representative RPE1 cell stably expressing Zyxin-GFP rounding up as it enters mitosis. 1 basal z-slice. Time is shown relative to NEP. Scale-bar 20  $\mu\text{m}$ . **(E)** Zoom of boxed region in (D) with 3 neighbouring adhesions highlighted as they are formed and eventually lost. Time is shown relative to NEP. Scale-bar 2  $\mu\text{m}$ . **(F)** RPE1 cells stably expressing Zyxin-GFP were released from CDK1 inhibition to synchronise entry into mitosis (see Materials and Methods). Picture shows a representative cell (from a sample of 15 cells from 3 experiments), imaged during rounding, which was fixed in metaphase and stained on the microscope to visualize actin (magenta) and integrins (yellow) using phalloidin TRITC and Integrin  $\beta 1$  antibody. 1 basal z-slice. Scale-bar 20 $\mu\text{m}$ . (See S1 for another sample cell which leaves cytoplasmic tails during mitosis). Image shows montage of the boxed region of the cell, overlaying the fixed integrin staining (yellow), with live Zyxin-GFP puncta loss (magenta). 1 basal z-slice. Scale-bar 20 $\mu\text{m}$ .

**Figure 2.** Integrin-based attachments, left at mitotic entry, aid daughter cell re-spreading at mitotic exit:

**(A)** Image depicts an RPE1 stably expressing Zyxin-GFP entering and then exiting mitosis. 1 basal z-slice. Time is shown relative to nuclear envelope permeabilisation (NEP). Scale-bar 20 $\mu$ m. **(B)** Image shows an overlay of the cell from (A) during interphase (-9min) and during re-spreading (+48min). **(C)** Images show a RPE1 cell transiently expressing  $\alpha$ V-Integrin-GFP in interphase, metaphase and telophase. Dotted line in first panel was used to generate the kymograph in the final panel. Arrows show a representative adhesion which is present during interphase, maintained during metaphase, and returned during telophase. Scale-bar 20 $\mu$ m. **(D)** Montage shows RPE1 cell stably expressing Zyxin GFP, exiting mitosis with 1 tail. Time is shown relative to anaphase. 1 basal z-slice. Scale-bar 20  $\mu$ m. **(E)** Graph shows the time from anaphase to the onset of re-spreading in daughter cells which either do or don't inherit a tail. Mean  $\pm$  SD. N=6 exp. Statistics used t test.

**Figure 3.** The importance of cell-substrate adhesion for RPE1 cell division:

**(A)** Montage showing phase and Tubulin-GFP expression in RPE1 cells showing cells fail to divide when imaged in non-adhesive PLL-PEG coated wells which force them to divide in suspension. Time is shown relative to anaphase. Wide-field image. Scale-bar 20 $\mu$ m. **(B)** Graph shows the percentage of RPE1 which succeed and fail division in adhesive and non-adhesive wells. N=2 experiments. Statistics used the Chi-square test. **(C)** Montage showing phase and LifeAct-RFP expression in HeLa cells imaged in non-adhesive PLL-PEG coated wells which force them to divide in suspension. Wide-field image. Scale-bar 20 $\mu$ m. **(D)** Graph shows the percentage of HeLa cells which succeed and fail division in adhesive and non-adhesive wells. N=1 experiment. Statistics used the Chi-square test. **(E)** Graph shows the percentage of RPE1 which

succeed and fail division on substrates of different stiffness. N=4 experiments. See S3C for montages of sample cells. Statistics used the Chi-square test.

**Figure 4.** Integrin based protrusions allow division in Ect2-depleted cells:

**(A)** Graph depicts the percent of cells which succeed or fail division in Control siRNA cells, Ect2 siRNA in 4 cell types; HeLa, MCF10A (N=2 experiments), RPMI and MDA-MB-231 (N=3 experiments). **(B)** Graph depicts the percent of RPE1 cells which succeed or fail division in Control siRNA cells, Ect2 siRNA cells without tails and Ect2 siRNA cells with tails. N=8 experiments. See also Figure S4I-J for comparable data with a ROCK inhibitor. **(C)** Images show RPE1 Control siRNA and Ect2 siRNA cells fixed and stained with phalloidin TRITC (magenta), Anillin (yellow), Tubulin (magenta) and p-Myosin (yellow) antibodies. DAPI is shown in blue in the merge. 1 medial z-stack. Scale-bar is 20 $\mu$ m. See also Figure S2B for Ect2 antibody staining. **(D)** Graphs quantifying of the loss of Actin (Statistics used t test), Anillin (Statistics used Mann-Whitney test) and pMyosin (Statistics used Mann-Whitney test) proteins from bridge connecting daughter cells, where the neck measures less than 5 $\mu$ m. For each cell a 10x10 px (1.1 x 1.1 $\mu$ m) square in the neck is normalised to the average intensity of two identical sized boxes in each daughter cell cytoplasm. Mean  $\pm$  SD. N=1 experiment. **(E)** Images depict sample cells treated with either Control or Ect2 siRNA stained for AuroraB (yellow) and Tubulin (magenta). Scale-bar is 20 $\mu$ m. Zoom of the boxed regions shows the midbody. Scale-bar is 2 $\mu$ m. **(F)** Graph showing time from anaphase to abscission in Control siRNA and Ect2siRNA cells. Mean  $\pm$  SD. N=7 experiments. Statistics used Mann-Whitney test.

**(G)** Montage of Control siRNA and Ect2 siRNA RPE1 cells stably expressing LifeAct-RFP as they exit mitosis. The magenta arrow shows the measurement taken over time

of decreasing neck width. The blue arrow shows the measurement taken over time of the increase in length between the polar leading edge of the two daughter cells as they migrate away from each other. The Ect2 RNAi cell depicted here re-spreads faster than the average. 5 $\mu$ m max projection of basal-medial cell. Scale-bar 20 $\mu$ m. See also Figure S3D for comparable data with a ROCK inhibitor. **(H)** Graphs depict the rate at which the width of the connection linking daughter cells decreases, and distance between daughter cell poles increases as cells divide. Data have been normalised to the first timepoint. **(I)** Graphs depict the mean rate at which the width of the connection linking daughter cells decreases, and distance between daughter cell poles increases as cells divide. Data have been normalised to the first timepoint. N=12 cells from 2 experiments. Error bars show SD.

**Figure 5.** Re-spreading of daughter cells is required for division in Ect2-depleted cells: **(A)** Montages showing Control siRNA and Ect2 siRNA cells plated on micro-patterned fibronectin discs surrounded by PLL-PEG. Dotted line denotes the pattern shape. Wide-field image. Scale-bar 20 $\mu$ m. **(B)** Graphs depicting the decreasing neck width and increasing length between the leading edges of daughter cells during division. **(C)** Graph showing the percentage of Ect2 siRNA cells which succeed and fail division on each pattern type. N=7 experiments. **(D)** Graph showing the length daughter cells had re-spread to by 21min after anaphase in Control siRNA and Ect2 siRNA cells which succeed or fail division. N=3 experiments. Median  $\pm$  interquartile range. Statistics used t test. **(E)** Graph showing the percentage of Ect2 siRNA cells with and without 300 $\mu$ M Arp2/3 inhibitor which succeed and fail division. N=4 experiments. Statistics used Chi-square test. **(F)** Graph showing the percentage of Control and Ect2 siRNA cells which succeed and fail division when re-plated from suspension at mitotic exit. N=4 technical

replicates from 1 experiment. Statistics used Chi-square test. **(G)** Graph showing the percentage of Control and Ect2 siRNA cells which succeed and fail division when plated on either fibronectin or PLL.

**Figure 6. Model:**

**(A)** A normal cell rounding, leaving integrin positive adhesive contacts before undergoing acto-myosin based cytokinesis using high Rho activity (\*). **(B)** A cell undergoing mitosis in suspension and either failing or succeeding to complete division depending on cell type. **(C)** A cell treated with Ect2 siRNA and either failing (I) or succeeding (II) to divide in a manner that depends on high Rac-Arp2/3 activity (\*\*).

## **STAR methods**

### **CONTACT FOR REAGENT AND RESOURCE SHARING**

Further information and requests for resources and reagents should be directed to and will be fulfilled by the Lead Contact Buzz Baum (b.baum@ucl.ac.uk).

### **EXPERIMENTAL MODEL AND SUBJECT DETAILS**

#### **Cell lines and culture**

hTERT-RPE1 (female) cells (Clontech) and MDA-MB-231 (female) cells (gift from E. Sahai) were cultured in DMEM F-12 Glutamax (Gibco 31331-028), with 10% fetal bovine serum, 3.4% sodium bicarbonate (Gibco 25080-060), 1% Penstrep (Gibco 15070-063). RPE1  $\alpha$ -tubulin-EGFP were a gift from D. Gerlich. RPMI-7951 (female) cells (purchased from the American Type Culture Collection (ATCC) Number: HTB-66) and HeLa (female) cells (MitoCheck (Hutchins et al., 2010)) were cultured in DMEM (Gibco 41965-039) with 10% FBS and 1% PenStrep. HeLa LifeAct-Ruby cells were made in lab by M. Fedorova. MCF10A (female) cells (gift from E. Sahai) were cultured in DMEM F-12 Glutamax, with 5% Horse serum (Invitrogen 16050), 20ng/ml

EGF (Peprotech 100-15R), 0.5mg/ml Hydrocortisone (Sigma H-0888), 100ng/ml Cholera toxin (Sigma C-8052), 10 $\mu$ g/ml Insulin (Sigma I-1882), 1% Penstrep. Leibovitz's L-15 CO<sup>2</sup> independent media (Gibco 21083-027) +10%FBS was also used during imaging. Cell lines have not been authenticated.

## **METHOD DETAILS**

### **Plasmid transfection**

rLV<sup>Ubi</sup>-LifeAct-TagRFP lentiviral vector (Ibidi 60142) was used to infect RPE1 cells. Positive cells were then selected with 1 $\mu$ g/ml puromycin to generate a stable cell line.

Plasmid transfection with the pArek1-EGFP-Zyxin plasmid (Gift from A. Welman (Welman et al., 2010)) was carried out using Fugene HD (Promega E2311). Positive RPE1 cells were selected with 500 $\mu$ g/ml G418 (Calbiochem 345812) to generate a stable cell line. Transient transfection of HeLa with H2B-mCherry, Talin-GFP (Franco et al., 2004), chicken Paxillin-GFP (Laukaitis et al., 2001) or Zyxin-GFP (Welman et al., 2010), pRK5-Rap1[Q63E] (Dupuy et al., 2005) was carried out with the same protocol.

$\alpha$ V-Integrin-GFP was a gift from R. Horwitz (Addgene plasmid # 15238) and was transiently transfected into RPE1 cells using Lipofectamine LTX and Plus reagent (Invitrogen 15338-100).

### **Ect2 siRNA**

siRNA treatment was carried out using AllStars negative control siRNA (Qiagen 1027280), Hs\_ECT2\_6 Flexitube siRNA (ATGACGCATATTAATGAGGAT-Qiagen SI03049249) and Lipofectamine RNAimax (Invitrogen 13778-075) diluted in optimem (Gibco 51985-026). Cells were used approximately 20 hours post-transfection.

### **Drug treatments**

Cells were incubated with 50 $\mu$ M of the small molecule Y27632 (Sigma Y0503) which inhibits ROCK activity and imaged the same day. Cells were incubated with 300 $\mu$ M

of the small molecule CK-666 (Sigma SML0006) which inhibits Arp2/3 activity and imaged immediately.

To synchronise cells prior to mitosis they were incubated with 9 $\mu$ M Ro-3306 (Enzolife Sciences ALX-270-463) to inhibit CDK1 activity for 15-20hours. This was replaced with drug free media immediately before imaging.

To synchronise cells in metaphase they were incubated with 10 $\mu$ M STLC (Sigma 164739) for 4hours. Then a mitotic shake off was carried out and the collected cells washed twice before being re-suspended in imaging media, re-plated and imaged immediately.

### **Micropatterning and surface treatment**

Standard experimental imaging was carried out on glass bottomed dishes incubated with 10 $\mu$ g/ml fibronectin for 1 hour at 37°C. Poly-L-Lysine (Sigma P4832) was incubated on a glass bottomed dish for 5 min room temperature with rocking, removed and allowed to air dry for 2 hours before seeding cells.

For micropatterning, HCL cleaned coverslips were passivated by plasma cleaning for 30seconds before incubating for 30min at room temperature with 0.1mg/ml PLL-g-PEG-633 (SuSoS PLL(20)-g[3.5]- PEG(2)/Atto633). A drop of MilliQ water was used to attach the coverslips to a quartz mask custom designed with the desired patterns and exposed to deep UV through the mask for 4min. The illuminated coverslip surface was then incubated for 1hour at room temperature with 25 $\mu$ g/mL of fibronectin (Sigma F1141) solution in 100mM NaHCO<sub>3</sub> pH 8.5 (Gibco 25080-060). Versene 1X (Gibco 15040-066) was used to dissociate cells before plating on coverslips to ensure fast re-spreading on patterns and cells were imaged within 4hours.

### **Wells**

40 $\mu$ m diameter PDMS wells were adhered to a plasma treated glass bottomed dish and baked at 75°C for 1hour before being incubated in 0.1mg/ml PLL-PEG (SuSoS PLL(20)-g[3.5]- PEG(2)) overnight. Cells were added to the well immediately prior to

imaging.

### **Cell fixation and immunostaining**

16% warmed PFA was added to cells in media to a final concentration of 4% and incubated at room temperature for 20min. Alternatively, 10% cold TCA was added and incubated at room temperature for 20min, or ice cold methanol was added and incubated at -20°C for 5 min. They were then washed 3 times and 0.2% Triton was added for 5min (only to PFA fixed cells, not TCA or methanol fixed). 5% bovine serum albumin/PBS was used to block for 30min at room temperature before primary antibodies were added. Activated Integrin  $\beta$ 1 (Abcam Cat# ab30394, RRID:AB\_775726), Paxillin (Abcam Cat# ab32084, RRID:AB\_779033), Talin (Sigma-Aldrich Cat# T3287, RRID:AB\_477572), Ect2 (Santa Cruz Biotechnology Cat# sc-1005, RRID:AB\_2246263), Anillin (Gift from C. Field (Hu et al., 2008)),  $\alpha$ -Tubulin (Sigma-Aldrich Cat# T9026, RRID:AB\_477593), p-Myosin LC2 Ser19 (Cell Signaling Technology Cat# 3671, RRID:AB\_330248) and AuroraB (Abcam Cat# ab2254, RRID:AB\_302923). Phalloidin Tritc (Sigma-Aldrich Cat# P1951, RRID:AB\_2315148) and DAPI (Thermo Fisher Scientific Cat# D3571, RRID:AB\_2307445) were added with secondary antibodies (Invitrogen 647 anti mouse or 448 anti rabbit).

Fixed samples were imaged on a Leica TCS SPE 2 microscope except for the online fixation experiment.

For online fixation RPE1 Zyxin-GFP CDK1 inhibited cells were imaged on a Nikon Eclipse Ti microscope with Andor Neo-Zyla camera. Using the pump system established by P. Almada (Almada, 2017), the media was exchanged at the microscope to remove inhibition and allow the cells to enter mitosis and imaging continued. 30min after media exchange when many cells were in metaphase, the PFA fixation protocol as above was triggered to fix and stain the cells at the microscope. The same cells were then imaged post fixation.

### **Live cell imaging**

Widefield imaging was carried out on Nikon Ti inverted microscope or a Zeiss

Axiovert 200M microscope at 3 or 5 minute timepoints using a 20x or 40x objective.

Live confocal imaging was carried out on a Nikon TiE inverted stand attached to a Yokogawa CSU-X1 spinning disc scan head, using the 40X objective and 3 minute timepoints.

### **Western blot**

Treated cells were lysed using chilled RIPA buffer on ice. The protein concentration of the supernatant was determined using Bradford reagent and samples were run on 4-12% Tris Bis gel (Invitrogen NW04122). Gels were then blotted and probed with Ect2 (Santa Cruz sc-1005) and  $\alpha$ -tubulin (Sigma T9026) primary antibodies, and anti-mouse and anti-rabbit HRP-conjugated secondary antibodies (Dako).

### **Preparation of polyacrylamide gels**

Glass-bottom dishes were activated by using a 1:1:14 solution of acetic acid/bis-silane (M6514, Sigma)/ethanol. The dishes were washed twice with ethanol and air-dried for 5 min. For 5kPa/1.5kPa/0.5kPa gels, a 500 $\mu$ l stock solution containing PBS, 93.3 $\mu$ l/62.5 $\mu$ l/50 $\mu$ l acrylamide 40% (A4058, SIGMA), 11 $\mu$ l/10 $\mu$ l/7.5 $\mu$ l bisacrylamide 2% (BP1404-250, FisherScientific), 2.5 $\mu$ l 10% APS diluted in water (Sigma A7460), 0.25 $\mu$ l TEMED (BioRad 161-0800) and 12 $\mu$ l of 200-nm-diameter red fluorescent carboxylate-modified beads (F8810, ThermoFisher) was prepared. A drop of 18  $\mu$ l was added to the centre of the glass-bottom dishes and the solution was covered with 18-mm-diameter glass coverslip. After polymerization, the coverslip was removed and gels were functionalized using sulfo-sanpah (102568-43-4). Briefly, 80 $\mu$ l drop of sulfo-sanpah was placed on the top of the polyacrylamide gel and activated by UV light for 3 min. Sulfo-sanpah was diluted in miliQ water to a final concentration of 2mg/ml from an initial dilution 50mg/ml kept at -80°. Then, gels were washed twice with miliQ water and once with PBS for 5min each. Afterwards, gels were incubated with 200 $\mu$ l of a fibronectin solution (0.01mg ml<sup>-1</sup>) overnight at 4°C.

## **QUANTIFICATION AND STATISTICAL ANALYSIS**

### **Traction microscopy**

Traction forces were computed using Fourier transform based traction microscopy with a finite gel thickness. Gel displacements between any experimental time point and a reference image obtained after monolayer trypsinization were computed using home-made particle imaging velocimetry software (Treat et al., 2009). The transmitted force was computed as the net traction force generated by each one of the daughter cells after anaphase (Labernadie et al., 2017).

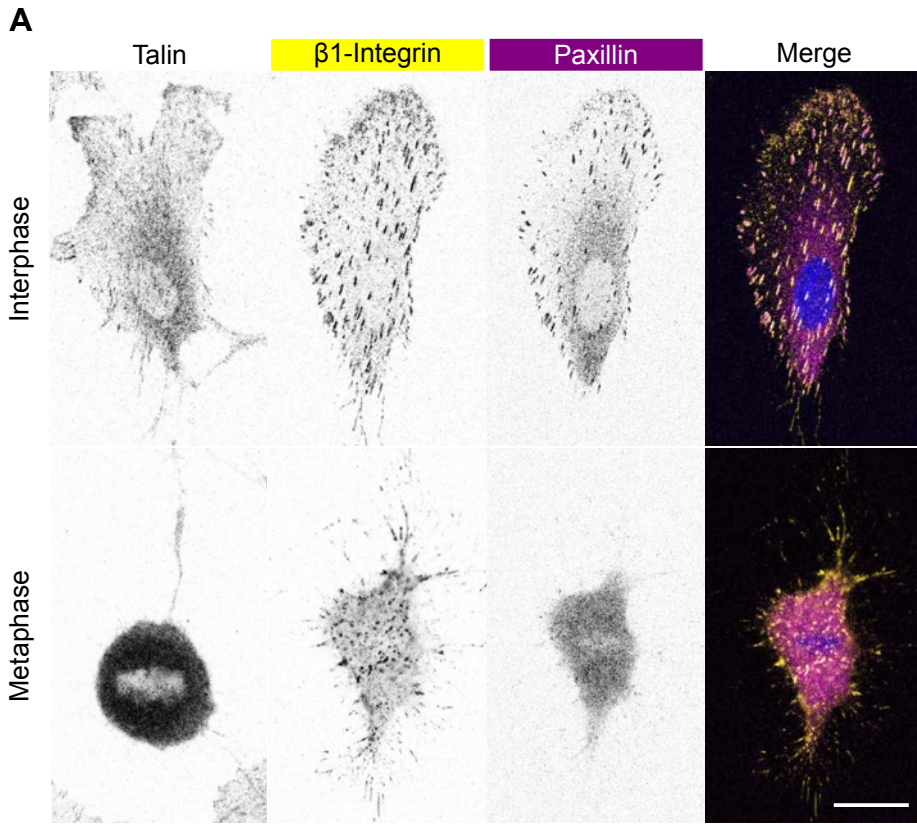
### **Statistical analysis**

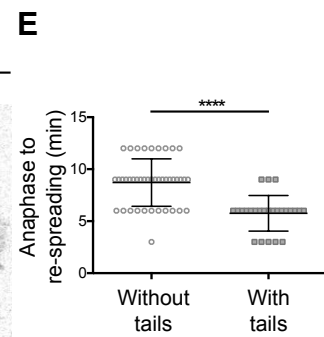
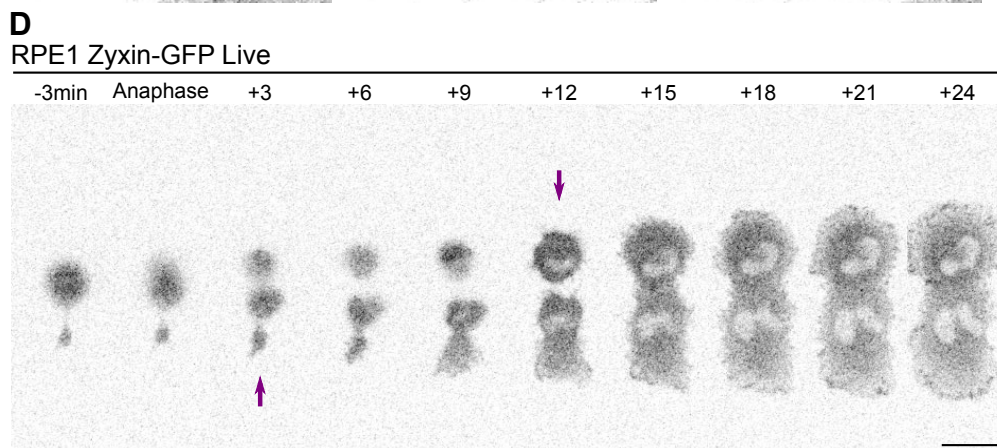
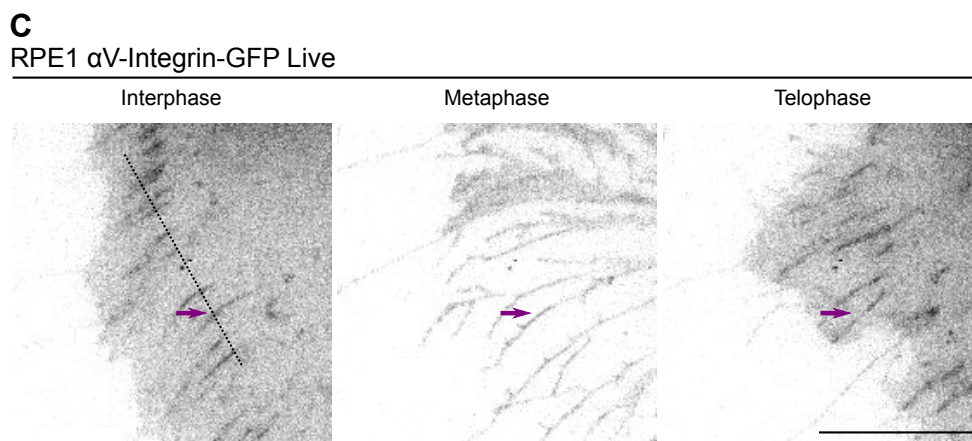
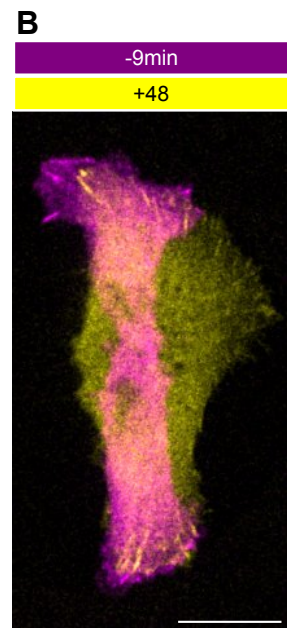
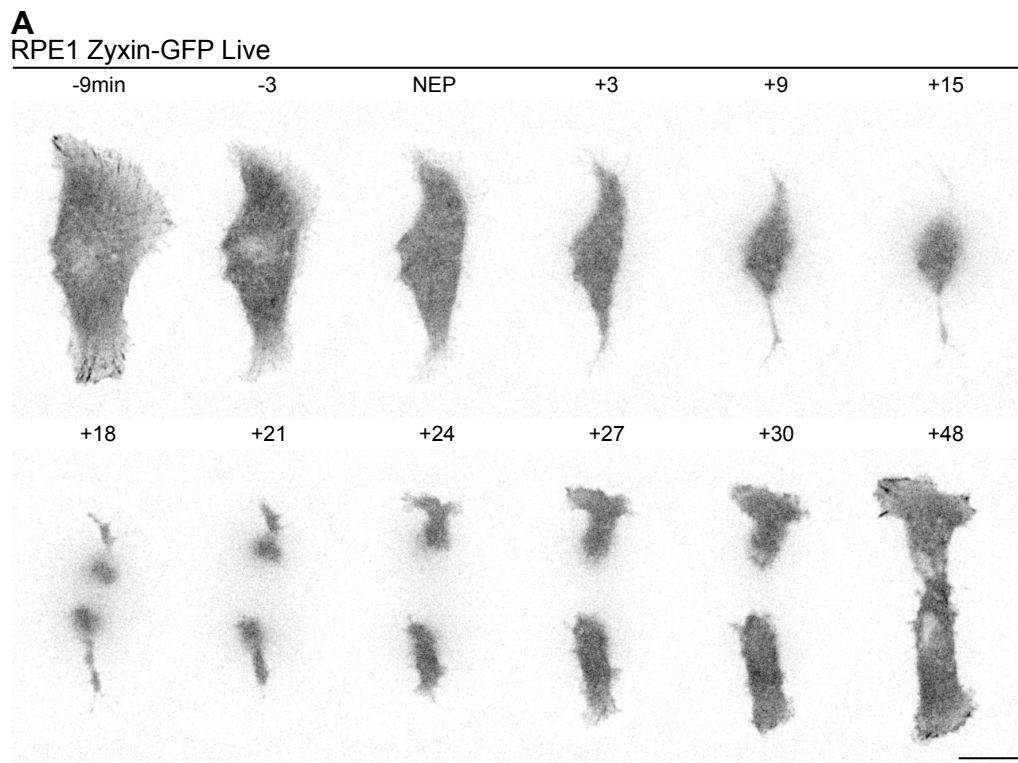
Apart from the traction force microscopy data, all analysis was carried out manually in Fiji. Graphs were produced in Microsoft Excel and Graphpad Prism. Statistical tests were carried out in Graphpad Prism. Normal data sets comparing distribution of values were analysed using the unpaired t test, two tailed. Non-normal data sets were analysed using Mann-Whitney two-tailed test. Binary data sets were analysed using the Chi-square test. \* $p < 0.01$  \*\* $p < 0.001$  \*\*\* $p < 0.0001$  \*\*\*\* $p < 0.00001$ . Details of the statistical tests used, exact value of n, definition error bars on graphs are all detailed for each figure in the legend.

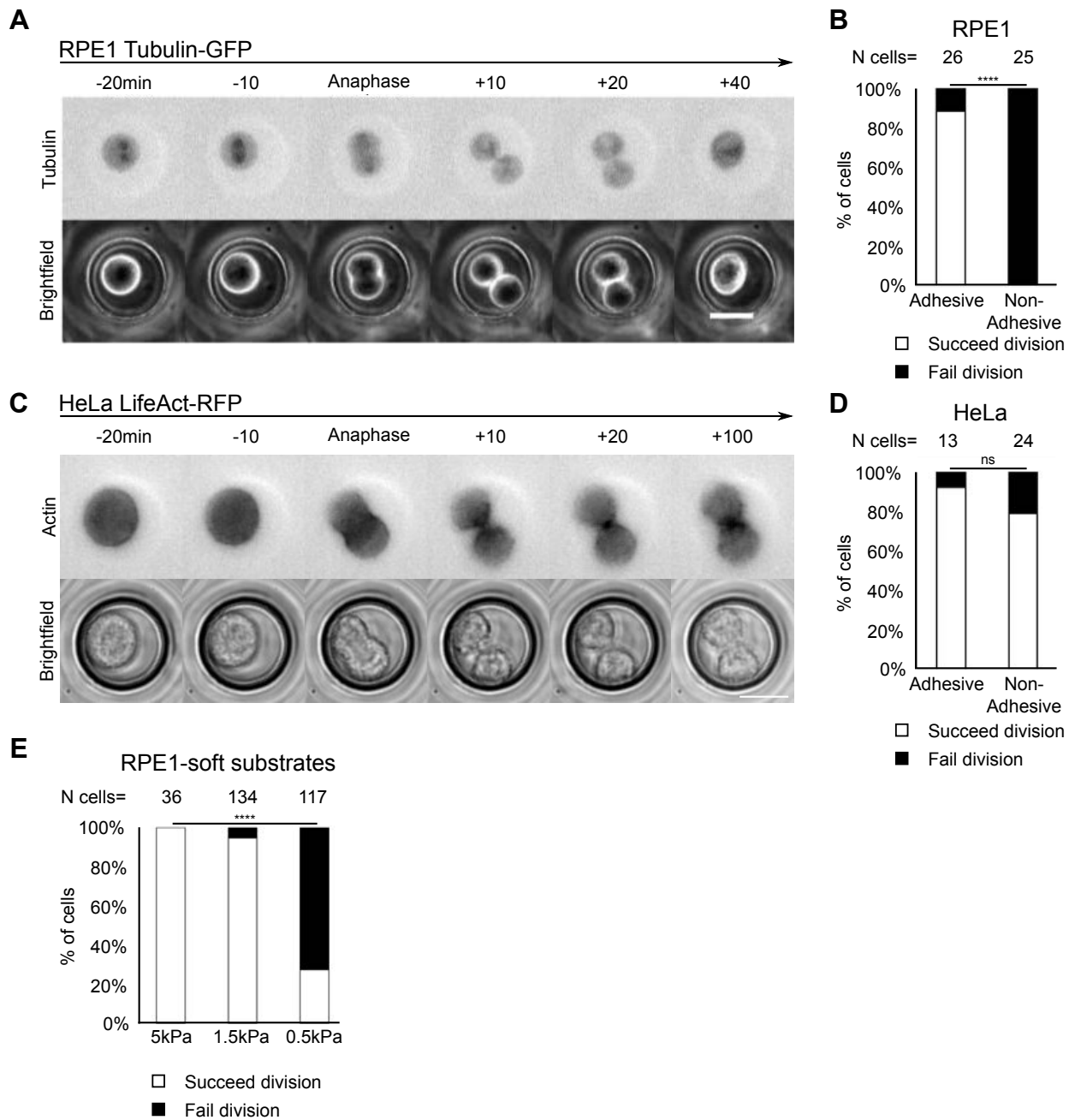
## KEY RESOURCES TABLE

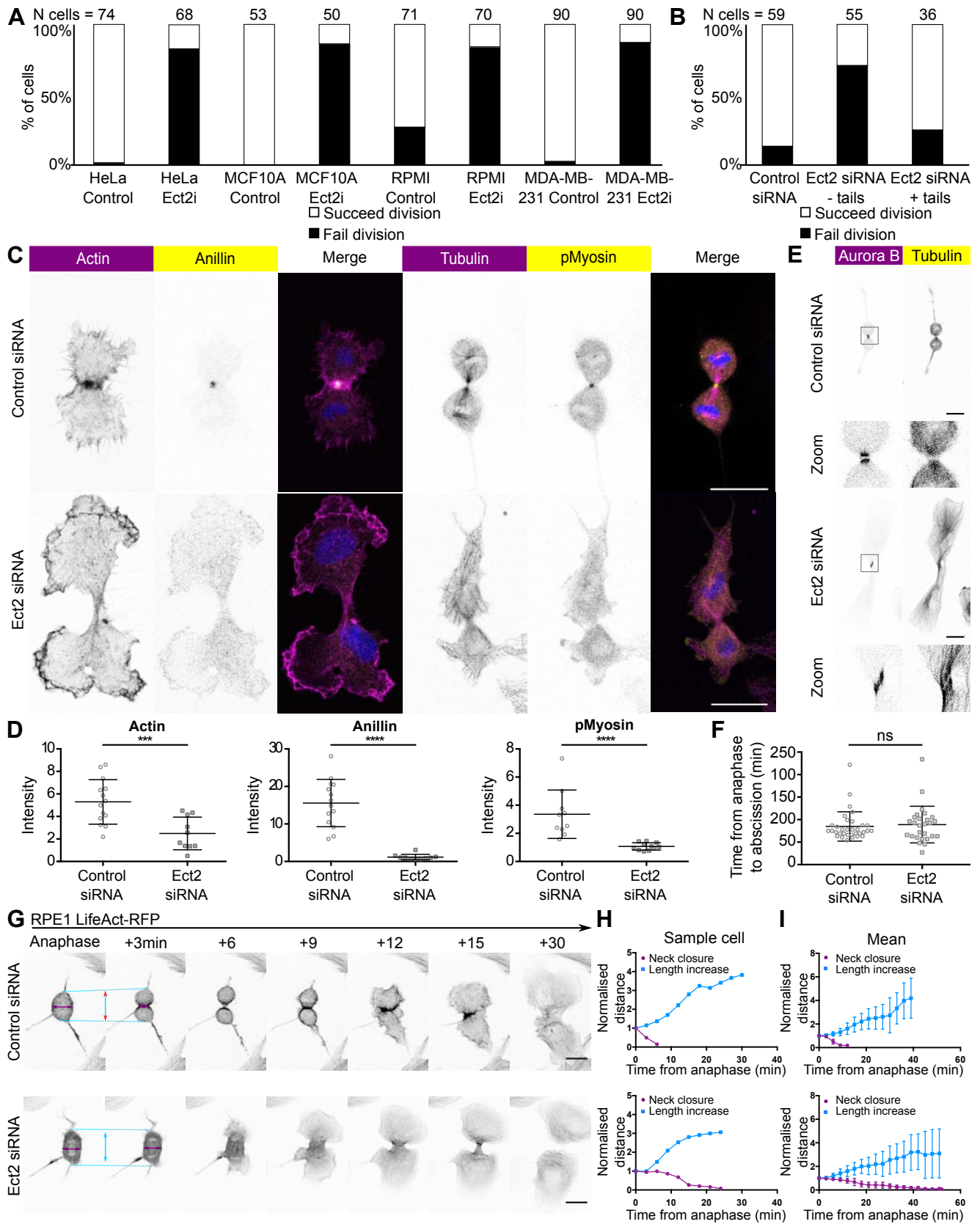
| REAGENT or RESOURCE                     | SOURCE   | IDENTIFIER   |
|---|--|--|
| <b>Antibodies</b>                       |  |  |
| Activated Integrin $\beta$ 1            | Abcam  | Abcam Cat# ab30394, RRID:AB_775726                     |
| Paxillin                                | Abcam  | Abcam Cat# ab32084, RRID:AB_779033                     |
| Talin                                   | Sigma  | Sigma-Aldrich Cat# T3287, RRID:AB_477572               |
| Ect2                                    | Santa Cruz   | Santa Cruz Biotechnology Cat# sc-1005, RRID:AB_2246263 |
| Anillin                                 | C. Field (Hu et al., 2008)                         | n/a  |
| $\alpha$ -Tubulin                       | Sigma  | Sigma-Aldrich Cat# T9026, RRID:AB_477593               |
| p-Myosin LC2 Ser19                      | Cell signaling technology                          | Cell Signaling Technology Cat# 3671, RRID:AB_330248    |
| AuroraB                                 | Abcam  | Abcam Cat# ab2254, RRID:AB_302923                      |
| Phalloidin TRITC                        | Sigma  | Sigma-Aldrich Cat# P1951, RRID:AB_2315148              |
| Dapi                                    | Invitrogen   | Thermo Fisher Scientific Cat# D3571, RRID:AB_2307445   |
| Ect2                                    | Santa Cruz   | Santa Cruz Cat# sc-1005, RRID:AB_2246263               |
| <b>Bacterial and Virus Strains</b>      |  |  |
| rLVUbi-LifeAct-TagRFP lentiviral vector | lbidi  | 60142  |
| <b>Experimental Models: Cell Lines</b>  |  |  |
| hTERT-RPE1                              | Clontech   | n/a  |
| RPE1 $\alpha$ -tubulin-EGFP             | D. Gerlich   | n/a  |
| MDA-MB-231                              | E. Sahai   | n/a  |
| RPMI 7951                               | American Type Culture Collection<br>Number: HTB-66 | ATCC Number: HTB-66                                    |
| HeLa Kyoto                              | MitoCheck (Hutchins et al., 2010)                  | n/a  |
| HeLa LifeAct Ruby                       | Made in lab by M. Fedorova                         | n/a  |
| MCF10A                                  | E. Sahai   | n/a  |

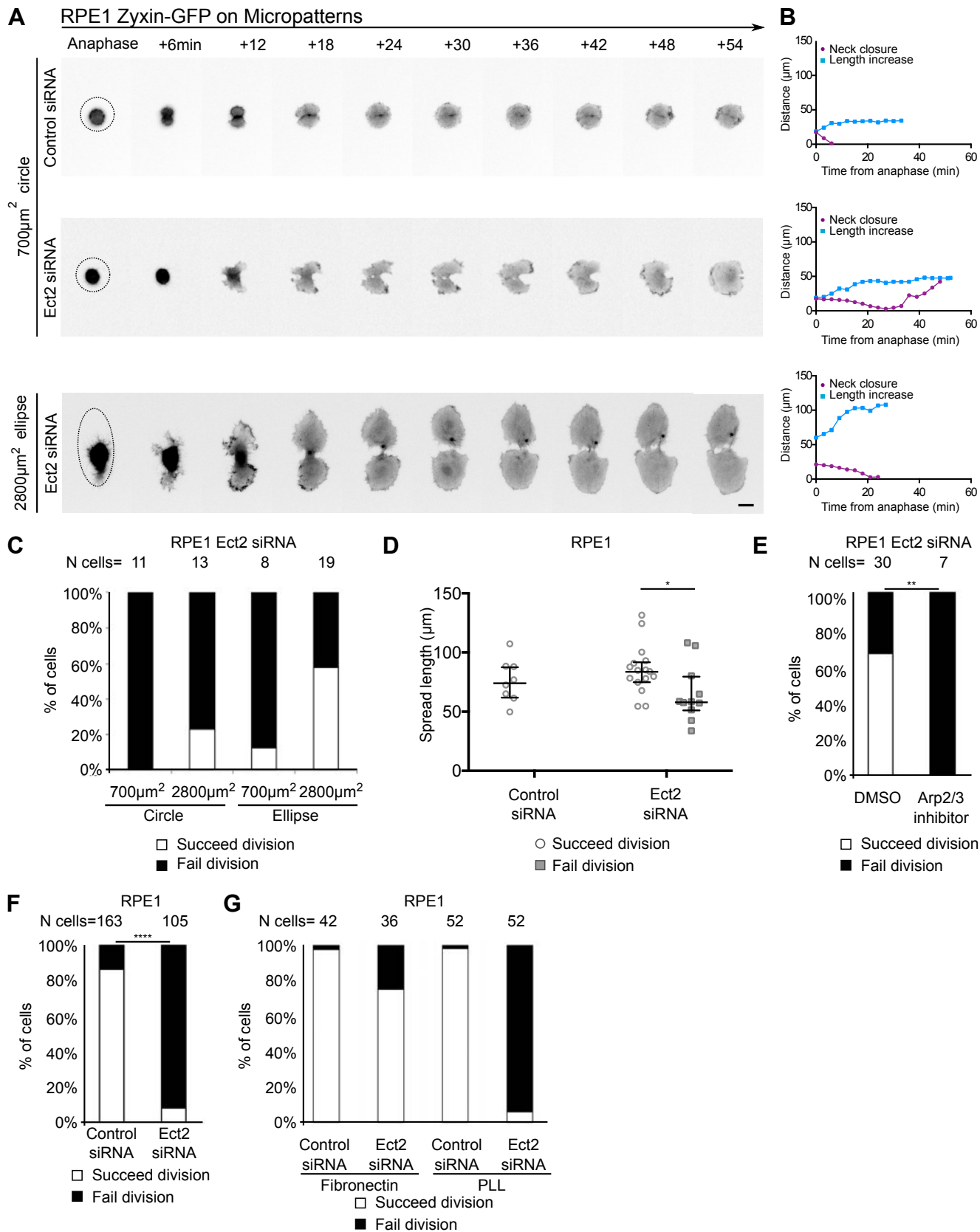
| Chemicals, Peptides, and Recombinant Proteins |  |                               |
|---|--|-------------------------------|
| Y27632  | Sigma  | Y0503                         |
| CK-666  | Sigma  | SML0006                       |
| Ro-3306                                       | Enzolife Sciences                                  | ALX-270-463                   |
| STLC  | Sigma  | 164739                        |
| PLL-g-PEG-633                                 | SuSoS  | PLL(20)-g[3.5]-PEG(2)/Atto633 |
| Fibronectin                                   | Sigma  | F1141                         |
| Versene 1X                                    | Gibco  | 15040-066                     |
| Experimental Models: Cell Lines               |  |                               |
| hTERT-RPE1                                    | Clontech   | n/a                           |
| RPE1 $\alpha$ -tubulin-EGFP                   | D. Gerlich   | n/a                           |
| MDA-MB-231                                    | E. Sahai   | n/a                           |
| RPMI 7951                                     | American Type Culture Collection<br>Number: HTB-66 | ATCC Number: HTB-66           |
| HeLa Kyoto                                    | MitoCheck (Hutchins et al., 2010)                  | n/a                           |
| HeLa LifeAct Ruby                             | Made in lab by M. Fedorova                         | n/a                           |
| MCF10A  | E. Sahai   | n/a                           |
| Recombinant DNA                               |  |                               |
| pAren1-EGFP-Zyxin plasmid                     | Welman et al., 2010                                | n/a                           |
| Talin-GFP                                     | Franco et al., 2004                                | n/a                           |
| pRK5-Rap1[Q63E]                               | Dupuy et al., 2005                                 | n/a                           |
| $\alpha$ V-Integrin-GFP                       | R. Horwitz   | Addgene plasmid # 15238       |
| chicken Paxillin-GFP                          | Laukaitis et al., 2001                             | n/a                           |
| Software and Algorithms                       |  |                               |
| Particle imaging velocimetry software         | Trepat et al., 2009                                |                               |
| Other   |  |                               |
| AllStars negative control siRNA               | Qiagen   | 1027280                       |
| Hs_ECT2_6 Flexitube siRNA                     | Qiagen   | SI03049249                    |





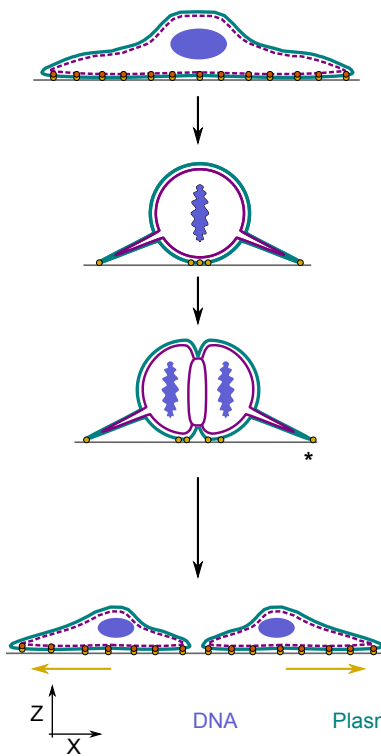






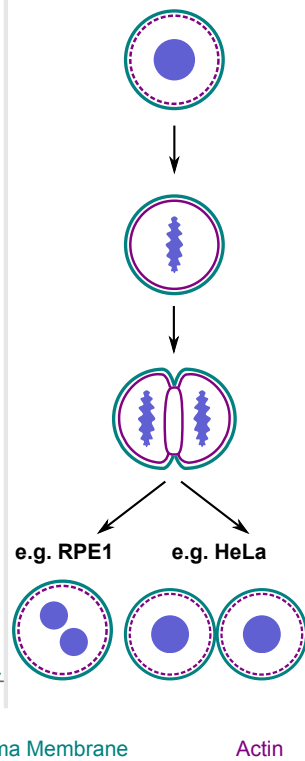
A

- ✓ Adhesion
- ✓ Contractility



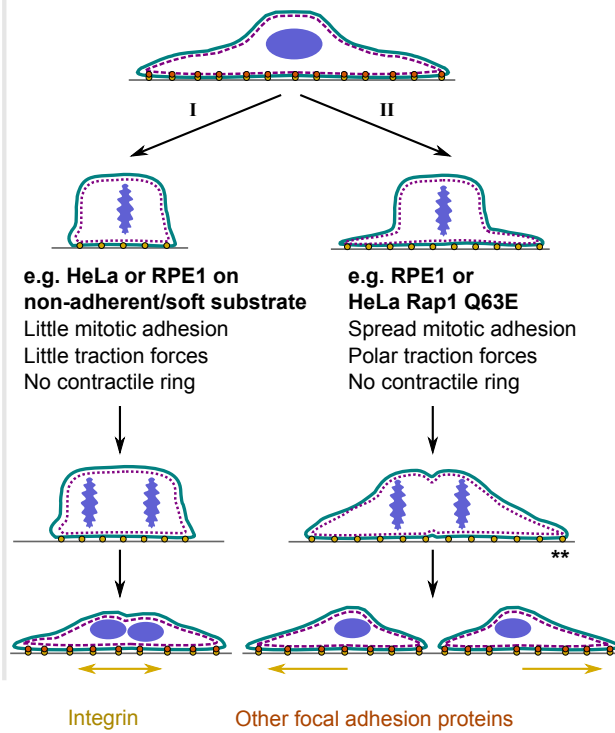
B

- ✗ Adhesion
- ✓ Contractility



C

- ✓ Adhesion
- ↓ Contractility



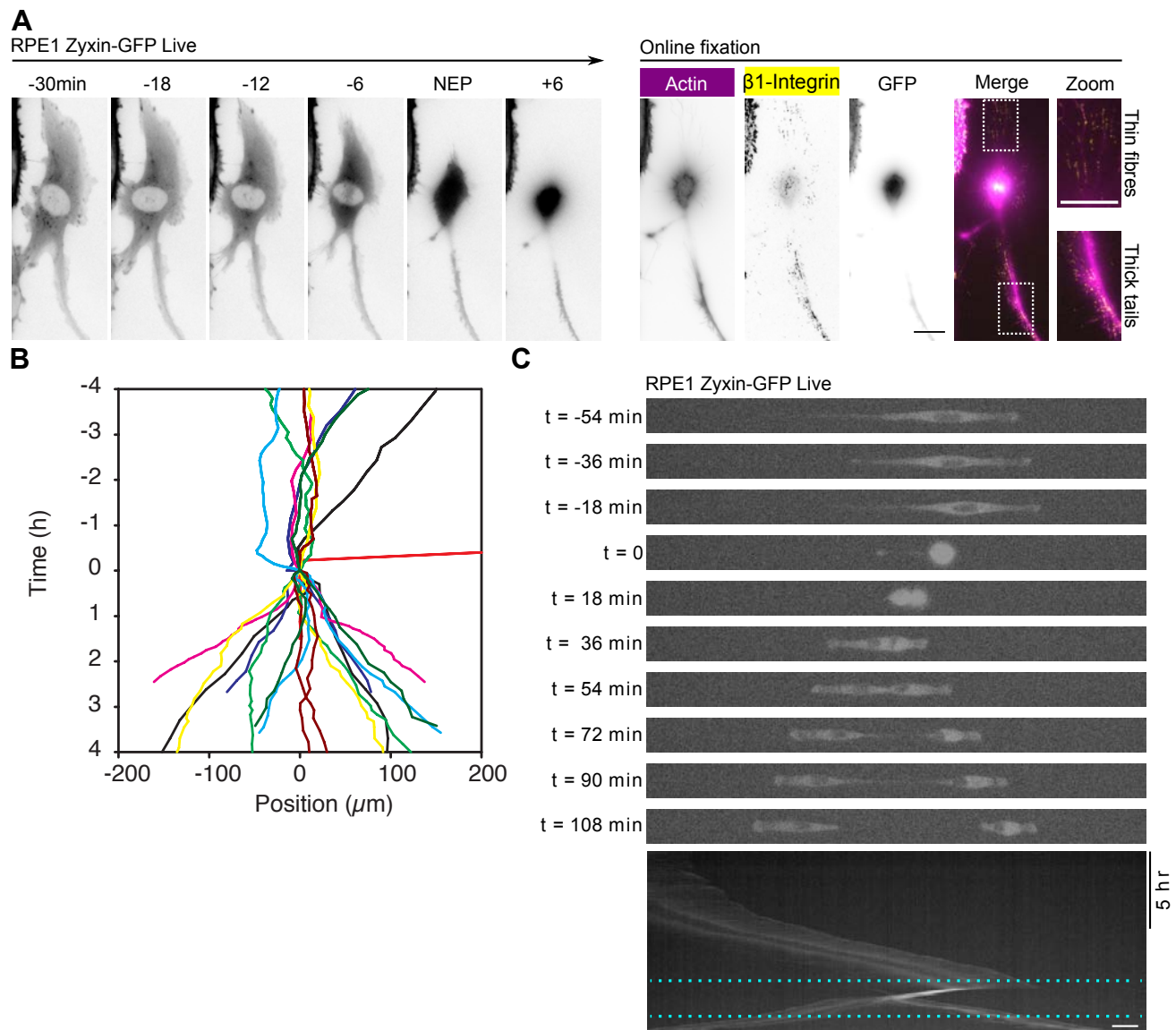


**Figure S2: Related to Figure 2**

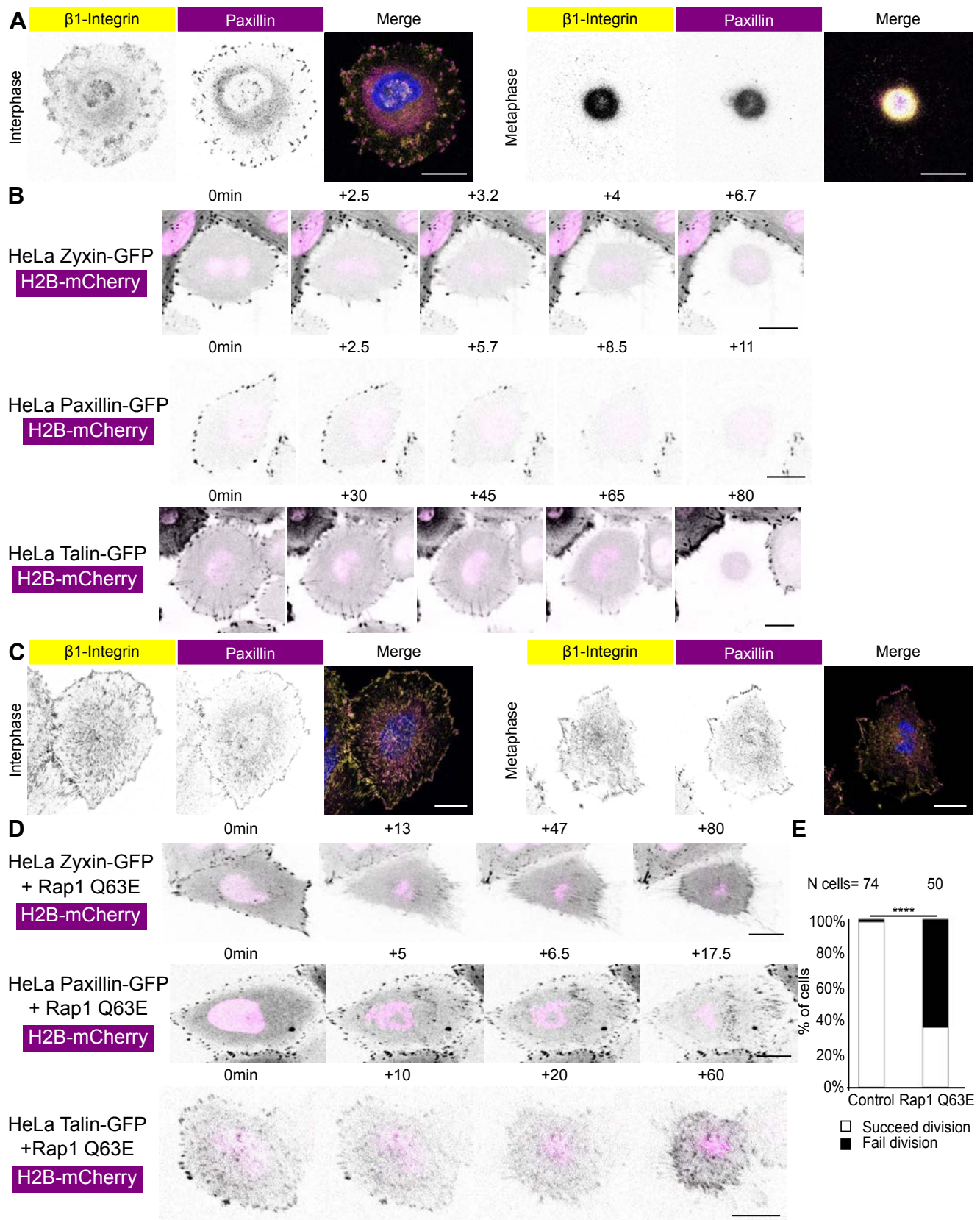
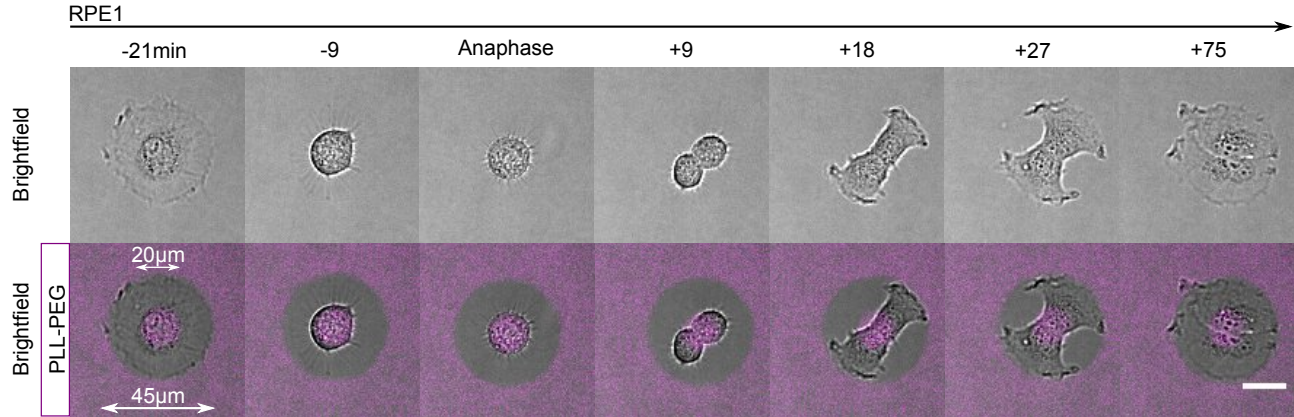
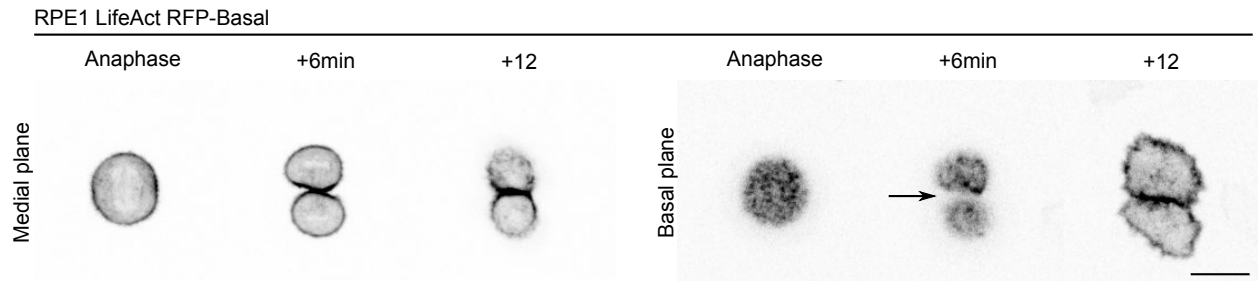


Figure S3: Related to Figure 3

**A**



**B**



**C**

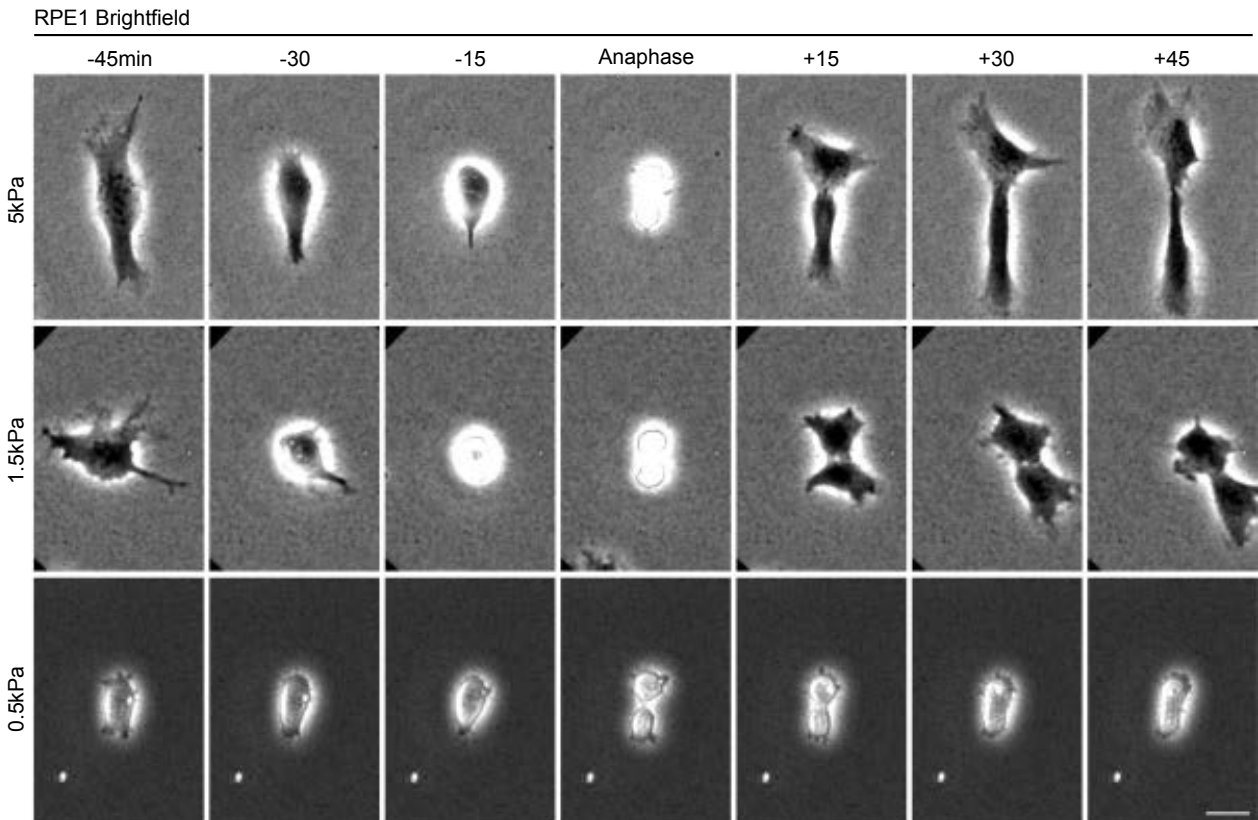


**Figure S4: Related to Figure 4**

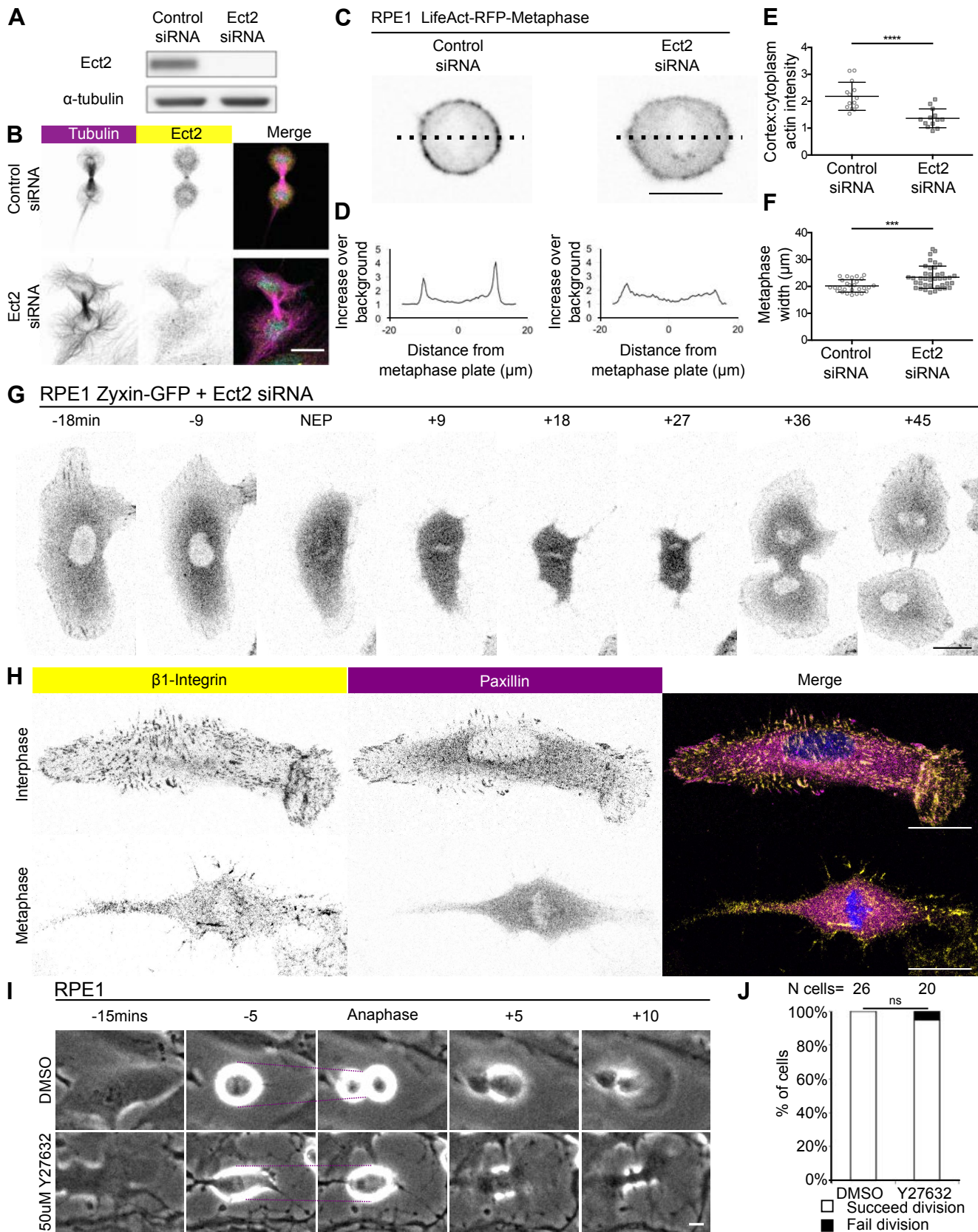
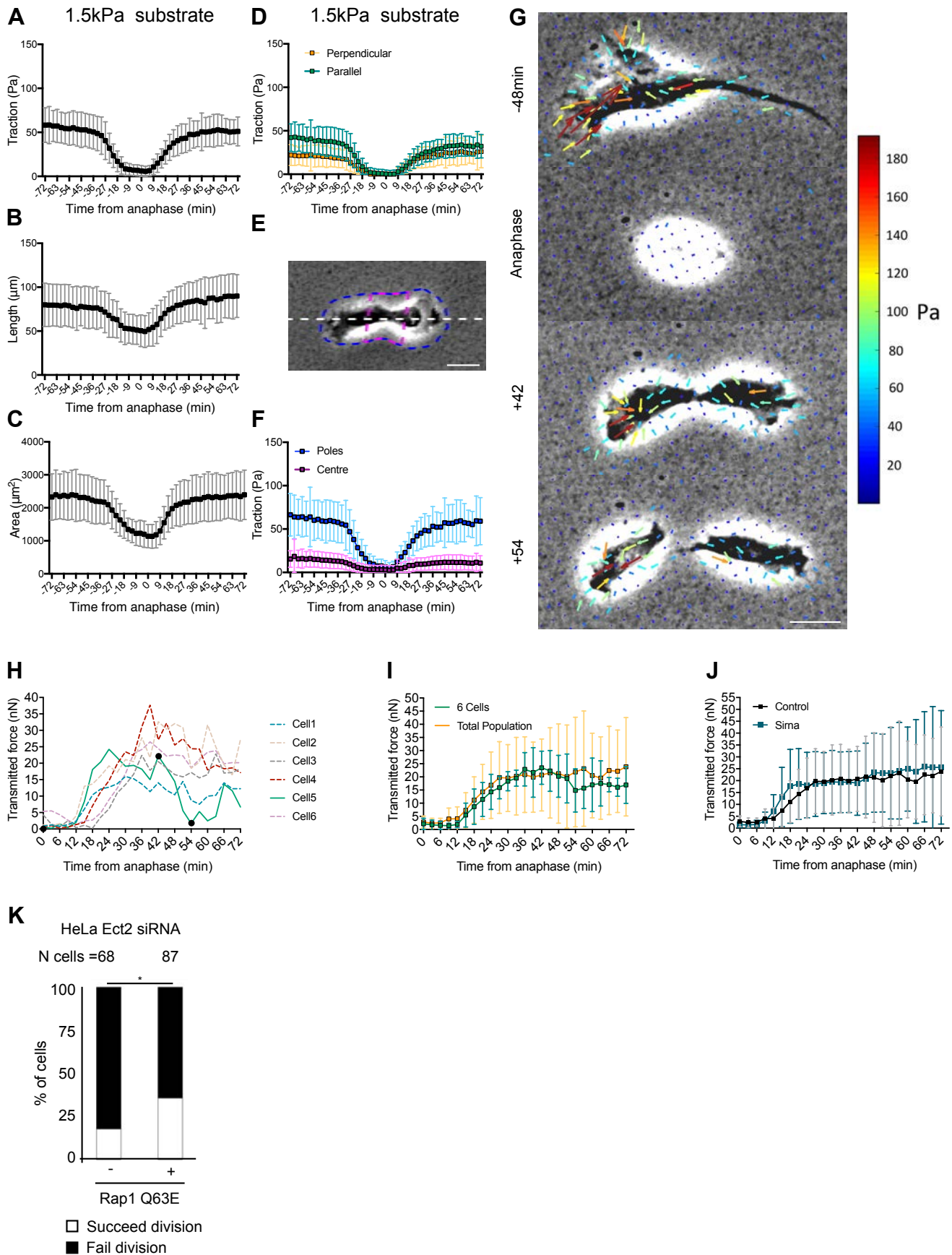


**Figure S5: Related to Figure 5**



## **Supplemental Figure legends**

### **Figure S1.** Related to Figure 1:

RPE1 cell stably expressing Zyxin-GFP imaged during rounding, then fixed in metaphase (as in 1G) and stained on the microscope to visualize DNA (cyan), actin (magenta) and integrin (yellow) using DAPI, phalloidin TRITC and active  $\beta$ 1-Integrin antibody. Zyxin-GFP remains visible after fixation. 1 basal z-slice. Scale-bar 20 $\mu$ m. Zooms of boxed regions show thin retraction fibres and an adhesive tail. **(B)** Graph quantifying RPE1 cells migrating on 20 $\mu$ m fibronectin lines. Each color represents an individual cell pre-mitosis and the two daughter cells post-mitosis. X-axis (position) and y-axis (time) set to 0 at metaphase. **(B)** Representative RPE1 Zyxin-GFP cell migrating on 20 $\mu$ m fibronectin line. Top: Montage shows fluorescent images of a subset of the kymograph between the blue dotted lines. Scale-bar 20 $\mu$ m. Bottom: Kymograph shows persistent RPE1 cell migration along the line before mitosis and daughter cells migrating in opposing directions after mitosis.

### **Figure S2:** Related to Figure 2:

**(A)** Images depict fixed HeLa cells in interphase and metaphase stained for active  $\beta$ 1-Integrin (magenta) and Paxillin (yellow). Merge also shows DAPI (blue). 1 basal z-slice. Scale-bar 20  $\mu$ m. **(B)** Montages show HeLa cells expressing H2B-mCherry and either Zyxin, Paxillin or Talin-GFP, entering mitosis and losing focal adhesion puncta. Scale-bar 20  $\mu$ m **(C)** Images depict fixed HeLa cells in interphase and metaphase transfected with Rap1[Q63E], stained for active  $\beta$ 1-Integrin (magenta) and Paxillin (yellow). Merge also shows DAPI (blue). 1 basal z-slice. Scale-bar 20  $\mu$ m. **(D)** Montages show HeLa cells transfected with Rap1[Q63E], expressing H2B-mCherry and either Zyxin, Paxillin or Talin-GFP, entering mitosis and losing focal adhesion

puncta. Scale-bar 20  $\mu\text{m}$ . **(E)** Graph showing the percent of HeLa cells which succeed or fail division with or without Rap1[Q63E]. N=2 experiments. Statistics used the Chi-square test.

**Figure S3.** Related to Figure 3:

**(A)** Montage showing phase in RPE1 cells imaged on fibronectin patterns with a non-adhesive hole in the centre. Time is shown relative to anaphase. Wide-field image. Merge shows the cell overlaid on the non-adhesive PLL-Peg signal, which is excluded from the fibronectin pattern. 11/11 cells from 3 experiments succeed division across a non-adhesive hole. Scale-bar 20 $\mu\text{m}$ . **(B)** Montage shows a representative RPE1 cell expressing LifeAct-RFP undergoing mitotic exit and lifting its furrow (arrow) off the substrate. Time is shown relative to anaphase. 1 medial and 1 basal z-slice. Scale-bar 20  $\mu\text{m}$ . Representative of 45 cells from 3 experiments. **(C)** Montages depict RPE1 cells progressing through mitosis on substrates of different stiffness. Scale-bar 20 $\mu\text{m}$ . See 3D for quantification of division fail rate.

**Figure S4.** Related to Figure 4:

**(A)** Western blot showing the extent of Ect2 silencing in RPE1 cells.  $\alpha$ -Tubulin antibody was used as a loading control. Representative of 2 experiments. **(B)** Images depict fixed Control siRNA and Ect2 siRNA RPE1 cells stained for  $\alpha$ -Tubulin (magenta) and Ect2 (yellow). The merge also shows DAPI (cyan). 1 z-slice in the medial plane. Scale-bar 20 $\mu\text{m}$ . **(C)** Images show Control siRNA and Ect2 siRNA treated RPE1 metaphase cells stably expressing LifeAct-RFP. 1 medial z-slice. Scale-bar 20 $\mu\text{m}$ . Dotted line shows measurement taken for figure S4D. **(D)** Line-graph showing the actin distribution in the medial plane of sample cells. Data have

been normalised to background. **(E)** Graph showing the ratio of actin intensity at the cortex compared to the cytoplasm in Control siRNA and Ect2 siRNA cells. For each cell, four square regions around the cortex were averaged and compared to the average of four square regions around the cytoplasm to create one data-point. N=2 experiments. Mean  $\pm$  SD. Statistics used t test. **(F)** Graph showing metaphase width of Control siRNA and Ect2 siRNA RPE1 cells. N=3 experiments. Mean  $\pm$  SD. Statistics used Mann-Whitney. **(G)** Montage showing a representative RPE1 Zyxin-GFP cell treated with Ect2 siRNA progressing through mitosis. Scale-bar 20 $\mu$ m. Zoom of boxed regions at -12min and NEP shows loss of puncta. Scale-bar 2 $\mu$ m. **(H)** Images show fixed Control siRNA and Ect2 siRNA cells stained with Paxillin antibody (magenta) and active Integrin- $\beta$ 1 antibody (yellow). Merge also shows Dapi. 1 basal z-slice. Scale-bar 20 $\mu$ m. **(I)** Montages showing RPE1 cells treated with DMSO or 50 $\mu$ M Y27632. Magenta line shows narrowing of the neck across 2 timepoints. Wide-field image. Scale-bar 20 $\mu$ m. **(J)** Graph showing the percent of cells which succeed or fail division in RPE1 cells treated with DMSO and 50 $\mu$ M Y27632. N=1 experiment. Statistics used Chi-square test.

**Figure S5.** Related to Figure 5:

**(A)** Graph showing the mean traction forces as cells enter and exit mitosis on a 1.5kPa substrate. Mean  $\pm$  SD. N= 43 cells from 4 experiments **(B)** Graph showing the mean length as cells enter and exit mitosis on a 1.5kPa substrate. Mean  $\pm$  SD. N= 43 cells from 4 experiments. **(C)** Graph showing the mean area as cells enter and exit mitosis on a 1.5kPa substrate. Mean  $\pm$  SD. N= 43 cells from 4 experiments. **(D)** Graph comparing the perpendicular and parallel traction forces (relative to the long axis of

the cell) as cells enter and exit mitosis on a 1.5kPa substrate. Mean  $\pm$  SD. N= 43 cells from 4 experiments. **(E)** Image shows how cells were gated to generate data for S5F. Scale-bar 20 $\mu$ m. **(F)** Graph comparing the traction forces at the centre and poles as cells enter and exit mitosis on a 1.5kPa substrate. Mean  $\pm$  SD. N= 43 cells from 4 experiments **(G)** Images show a cell on a 1.5kPa substrate progressing through mitosis and division. Arrows depict traction forces according to the heat scale on the right. Scale-bar 20 $\mu$ m. **(H)** Graph showing the transmitted force between daughter cells in 6 sample cells as they exit mitosis on a 1.5kPa substrate. Cell5 (green line), is the cell portrayed in (G), black dots represent the stills from (G). **(I)** Graph showing the mean transmitted force between daughter cells as they exit mitosis on a 1.5kPa substrate, in the 6 cells from (H), and in the general population. Mean  $\pm$  SD. N= 42 cells from 4 experiments. **(J)** Graph showing the mean transmitted force between daughter cells as they exit mitosis on a 1.5kPa substrate in Control siRNA (data as in (I)) and Ect2 siRNA cells. Mean  $\pm$  SD. Ect2 siRNA: N= 28 cells from 4 experiments. **(K)** Graph showing the percent of HeLa cells which succeed or fail division with or without Ect2 siRNA in combination with Rap1[Q63E]. N=3 experiments. Statistics used Chi-square test.